TU/e EINDHOVEN UNIVERSITY OF TECHNOLOGY

A two-mechanism and multiscale compatible approach for solid state electrolytes of (Li-ion) batteries

Citation for published version (APA):
Cabras, L., Danilov, D., Subber, W., Oancea, V., & Salvadori, A. (2022). A two-mechanism and multiscale compatible approach for solid state electrolytes of (Li-ion) batteries. *Journal of Energy Storage*, *48*, Article 103842. https://doi.org/10.1016/j.est.2021.103842

Document license:
TAVERNE

DOI:
10.1016/j.est.2021.103842

Document status and date:
Published: 01/04/2022

Document Version:
Publisher's PDF, also known as Version of Record (includes final page, issue and volume numbers)

Please check the document version of this publication:

• A submitted manuscript is the version of the article upon submission and before peer-review. There can be important differences between the submitted version and the official published version of record. People interested in the research are advised to contact the author for the final version of the publication, or visit the DOI to the publisher's website.
• The final author version and the galley proof are versions of the publication after peer review.
• The final published version features the final layout of the paper including the volume, issue and page numbers.

Link to publication

General rights
Copyright and moral rights for the publications made accessible in the public portal are retained by the authors and/or other copyright owners and it is a condition of accessing publications that users recognise and abide by the legal requirements associated with these rights.

• Users may download and print one copy of any publication from the public portal for the purpose of private study or research.
• You may not further distribute the material or use it for any profit-making activity or commercial gain
• You may freely distribute the URL identifying the publication in the public portal.

If the publication is distributed under the terms of Article 25fa of the Dutch Copyright Act, indicated by the "Taverne" license above, please follow below link for the End User Agreement:

www.tue.nl/taverne

Take down policy
If you believe that this document breaches copyright please contact us at:

openaccess@tue.nl

providing details and we will investigate your claim.

Download date: 05. Oct. 2023

Journal of Energy Storage 48 (2022) 103842

Contents lists available at ScienceDirect

Journal of Energy Storage

journal homepage: www.elsevier.com/locate/est

Research papers

A two-mechanism and multiscale compatible approach for solid state electrolytes of (Li-ion) batteries

L. Cabras [a], D. Danilov [b,c], W. Subber [d], V. Oancea [e], A. Salvadori [a,*]

[a] Dipartimento di Ingegneria Meccanica e Industriale, Università di Brescia, Italy
[b] Eindhoven University of Technology, P.O. Box 513, 5600 MB Eindhoven, The Netherlands
[c] Forschungszentrum Jülich, Fundamental Electrochemistry (IEK-9), D-52425 Jülich, Germany
[d] GE Research, Niskayuna, NY 12309, United States
[e] Dassault Systemes Simulia Corp, United States

ARTICLE INFO

Keywords:
Modeling and simulations
Solid electrolytes
Sensitivity analysis
Model validation

ABSTRACT

All-solid-state batteries are claimed to be the next-generation battery system, in view of their safety accompanied by high energy densities. A new advanced, multiscale compatible, and fully three-dimensional model for solid electrolytes is presented in this note. The response of the electrolyte is profoundly studied theoretically and numerically, analyzing the equilibrium and steady-state behaviors, the limiting factors, as well as the most relevant constitutive parameters according to the sensitivity analysis of the model, the novel model is finally validated in accordance with experimental results.

1. Introduction

All solid state batteries (SSBs) are claimed to be the next-generation battery system, since they combine superior thermal as well as electrochemical stability and avoid hazardous liquid electrolyte leakage [1,2]. As pointed out extensively in [3], however, SSBs are affected by a number of chemical and stability issues. In spite they have been mostly investigated experimentally, digital twins can guide and even partially replace experimental campaigns. Computational simulations *easily and rapidly* allow selecting constituents and tailoring architectures, providing meaningful insights on the evolution of ionic concentrations during operation [4–7] and predicting limiting factors together with material degradation in SSBs charge/discharge cycles [3,8–10].

At standard conditions, some of the Li ions in a solid electrolyte are thermally excited. Chemical ionization reactions occur, leaving behind uncompensated negative charges, associated with a vacancy in the matrix at the place formerly occupied by lithium. In most cases, see e.g. [11] and the references therein, the ionic transfer is described by a *single ion conduction model*. Since the negative vacancies in the lattice are modeled as firmly held, they cannot flow and the resulting concentration of Li ions across the solid electrolyte is uniform and known a priori in view of the electroneutrality [12]. Because no concentration gradient drives the ionic motion, those models reproduce essentially Ohm's law.

More recently, single ion conduction models have been displaced by *two-mechanism models*, which describe more realistically the ionic motility in solid electrolytes as due to hopping and interstitial diffusion. One-dimensional mathematical models for Lithium phosphorus oxynitride (LiPON henceforth) have been published in [13–15].

In this note, we propose a novel model of the ionic transport in solid electrolytes. It is set in a rigorous thermodynamics framework and accounts for the hopping/interstitial mechanisms and their interactions during batteries operations [16]. Profound theoretical and numerical investigations of the response of the electrolyte are here provided, analyzing the equilibrium and steady state behaviors, the limiting factors of the model, as well as the sensitivity of the ionic response to the most relevant constitutive model parameters. The model accounts for the electric field by means of the quasi-static Ampere–Maxwell equations, in order to ensure the multiscale compatibility, as largely described in [17]. Whereas the model is fully three-dimensional by nature, a whole cell one-dimensional FEM code has been built to the aim of validation against experimental evidences published in [18]. In that implementation, *interfaces mechanisms* have been accounted for: intermediate electrode/electrolyte layers have been modeled as interfaces between electrodes and the solid electrolyte, in terms of potential jumps as for plate capacitors [19]. Stemming from rigorous thermodynamic setting, conditions of non Butler–Volmer type arise [20].

The model published in [15] inspired this study, which is grounded in the thermo-mechanics of continua. The proposed formulation develops further the theory in [15], where both interstitial lithium and negative vacancies were allowed to flow, thus creating a concentration

* Corresponding author.
E-mail address: alberto.salvadori@unibs.it (A. Salvadori).

https://doi.org/10.1016/j.est.2021.103842
Received 6 July 2021; Received in revised form 7 October 2021; Accepted 14 December 2021
Available online 13 January 2022
2352-152X/© 2021 Elsevier Ltd. All rights reserved.

gradient at steady state that resembles the liquid electrolyte distributions found for instance in [17,21]. Depicting vacancies with the same conceptual framework used for negative ions in liquid electrolytes, i.e. as able to move in the solid matter with an entropic brownian motion together with migration within an electric field, does not appear to be physically sound. Accordingly, we reformulate the process of vacancies replenishment and make it multi-scale-compatible, which appears to be relevant for composite cathodes [6,7,22]. In our formulation, we model explicitly the dynamic filling of vacancies by neighboring positions, a motion of positive ions which in turn creates new vacancies. To this aim, we claim that after the ionization reactions occur, some ions hop and fill neighboring vacancies, whereas the remaining positive ions move in a meta-stable interstitial state. In this way, positive ions are the only moving species and the concentration of negatively charged vacancies results from the solution of the governing equations. Such a set of partial differential equations – mass balance equations, chemical kinetics laws, balance of momentum, and Ampere's law – is detailed in Section 2. Those continuity equations shall be supplied with constitutive laws, which arise from a rigorous thermodynamic analysis formulated in Section 3.

The steady state response of the system as well as the transient path of the unknown fields when initial conditions are far from equilibrium, a typical situation in real batteries, are retrieved via numerical simulations with the finite element method (FEM) (see Section 6.3).

Governing equations can be solved rather straightforwardly at steady state as well as at equilibrium: the closed form solutions highlight the role of material parameters, some of which can be measured only with major uncertainties. The sensitivity analysis (SA) helps in identifying model parameters that contribute the most to the prediction, and thus identifying the accuracy required in measuring these parameters [23]. The SA carried out in Section 7 allows to figure out the effect of the variability of model parameters on the variability of its prediction. The SA suggests that the fraction of Li that resides in equilibrium in the mobile state is the most sensitive parameter.

2. Electrochemical modeling of the solid electrolyte

The version of the model detailed in what follows is a restriction of a broader multi-physics formulation, which includes mechanical and thermal interactions according to [24]. Since the present note focuses on the electrochemical performance, for the sake of conciseness we assume both thermal and mechanical equilibrium, with relevant fields fixed during electrolyte operation.

2.1. Chemical kinetics

The amorphous structure of the LiPON electrolyte is schematically shown in Fig. 1. It highlights two types of nitrogen bonds, either triply- or doubly coordinated. Li_0 denotes the (ionic) lithium bound to the non-bridging oxygen atoms, Li^+ is a lithium ion and n^- is the uncompensated negative charge associated with a vacancy formed in the LiPON matrix at the place where Li^+ was originally bound. The maximal concentration of host-sites, denoted with c_0, is established by the stoichiometric composition of the electrolyte material. It is reached in the ideal case of absolute zero temperature, when all available host sites are fully filled with lithium ions and the ionic conductivity vanishes because all ions are immobile, see Fig. 1a. In standard conditions, see Fig. 1b, some of the Li-ions are thermally excited and the chemical ionization reaction

$$\mathrm{Li}_0 \underset{k_b^{\mathrm{ion}}}{\overset{k_f^{\mathrm{ion}}}{\rightleftarrows}} \mathrm{Li}^+ + n^- \tag{1}$$

occurs, k_f^{ion} and k_b^{ion} being the forward and backward rate constants for the ionization (or recombination) reaction, respectively. Their ratio is the equilibrium constant of reaction (1)

$$K_{\mathrm{eq}}^{\mathrm{ion}} = \frac{k_f^{\mathrm{ion}}}{k_b^{\mathrm{ion}}}. \tag{2}$$

The ionization reaction (1) leaves behind uncompensated negative charges, which are associated to a vacancy in the LiPON matrix at the place formerly occupied by lithium. In [15] those vacancies were modeled with the same conceptual formalism used for negative ions in liquid electrolytes, i.e. as able to move in the solid matter driven by an entropic Brownian motion together with migration within an electric field. Here, we attempt to explicitly account for the dynamic filling of vacancies by neighboring positions, where new vacancies are created. To this aim, we claim that after the chemical ionization reaction (1) occurs, some ions, denoted henceforth with $\mathrm{Li}^+_{\mathrm{hop}}$, hop and fill neighboring vacancies, whereas the remaining Li^+ ions move in a meta-stable interstitial state. This dynamic behavior is described by a further reaction, that converts part of the full amount of ions made available by reaction (1) into hopping lithium with the ability to fill vacancies, leaving to the remaining ions the interstitial motion responsibility :

$$\mathrm{Li}^+ \underset{k_b^{\mathrm{hop}}}{\overset{k_f^{\mathrm{hop}}}{\rightleftarrows}} \mathrm{Li}^+_{\mathrm{hop}} . \tag{3}$$

The ratio between k_f^{hop} and k_b^{hop}, which are the rate constants for reaction (3), is the equilibrium constant of that reaction

$$K_{\mathrm{eq}}^{\mathrm{hop}} = \frac{k_f^{\mathrm{hop}}}{k_b^{\mathrm{hop}}}. \tag{4}$$

In summary, reaction (1) makes lithium ions capable of unbinding from the non-bridging oxygen atoms and move within the complex amorphous LiPON structure, either by filling neighboring vacancies or by flowing interstitially. The proportion of ions in these two mechanisms is governed by reaction (3). When $k_f^{\mathrm{hop}} = 0$, no hopping mechanism is accounted for. As k_f^{hop} increases, since more interstitial lithium is depleted in favor of hopping, more vacancies are formed in the ionization reaction (1) thus favoring the hopping mechanism.

Concentrations c_α express the *molarity* (i.e. the number of moles per unit volume) of a generic species α: c_{Li^+} and $c_{\mathrm{Li}^+_{\mathrm{hop}}}$ denote the concentration of mobile Li ions, c_{Li_0} the concentration of immobile lithium, and c_{n^-} the concentration of uncompensated negative charges. The mass flux, i.e. the number of moles of species α measured per unit area per unit time, is denoted with $\vec{h}_\alpha$. Scalar and vector fields are defined in space $\vec{x} \in V$ and time $0 \le t \le t_f$. Functional dependence, however, is specified when necessary only to enhance readability.

For ideal systems, in which chemical potentials have entropy and energy contributions only, the chemical kinetics of reactions (1) and (3) are modeled via the law of mass action [25]:

$$w = k_f^{\mathrm{ion}} \frac{\theta_{\mathrm{Li}_0}}{1-\theta_{\mathrm{Li}_0}} - k_b^{\mathrm{ion}} \frac{\theta_{\mathrm{Li}^+}}{1-\theta_{\mathrm{Li}^+}} \frac{\theta_{\mathrm{n}^-}}{1-\theta_{\mathrm{n}^-}} , \tag{5}$$

where θ_α is the dimensionless ratio

$$\theta_\alpha = \frac{c_\alpha}{c_\alpha^{sat}}$$

and c_α^{sat} is the saturation limit of the generic species α. In diluted conditions, i.e. $\theta_\alpha \ll 1$, Eq. (5) writes

$$w = k_f^{\mathrm{ion}}\, c_{\mathrm{Li}_0} - k_b^{\mathrm{ion}}\, c_{\mathrm{Li}^+}\, c_{\mathrm{n}^-} , \tag{6a}$$

with a small abuse of notation on the kinetic constants. The reaction rate of the interstitial-hopping transformation is

$$y = k_f^{\mathrm{hop}}\, c_{\mathrm{Li}^+} - k_b^{\mathrm{hop}}\, c_{\mathrm{Li}^+_{\mathrm{hop}}} . \tag{6b}$$

As observed in [24] for the elastic and swelling contributions, electric potential may affect the kinetics of reaction and hence the law of mass action. Consistently with [24] and the Arrhenius formalism, it is proposed here that factors k_f and k_b in Eqs. (6a), (6b) are function of the electric potential ϕ in the following way:

$$k_f^{\mathrm{ion}} = k_{f_0}^{\mathrm{ion}}\, e^{\frac{\zeta F \phi}{RT}} , \qquad k_f^{\mathrm{hop}} = k_{f_0}^{\mathrm{hop}}\, e^{\frac{\zeta F \phi}{RT}} , \tag{6c}$$

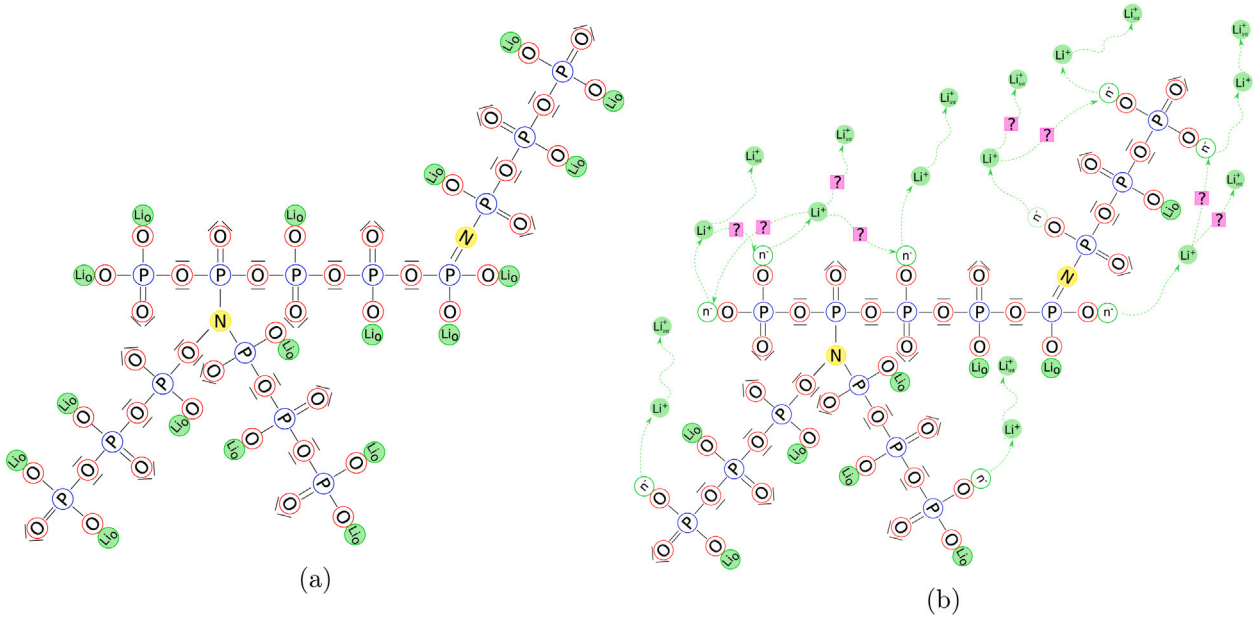

Fig. 1. LiPON matrix with triply- and doubly coordinated nitrogen (a). Movements of charged particles towards the interstitial space and by means of particle hopping, representing the main ionic conductivity mechanisms in LiPON (b).

$$k_b^{\text{ion}} = k_{b_0}^{\text{ion}}\, e^{\frac{\zeta F\phi}{RT}}\,, \qquad k_b^{\text{hop}} = k_{b_0}^{\text{hop}}\, e^{\frac{\zeta F\phi}{RT}}\,, \tag{6d}$$

with $R = 8.31446\,\text{J K}^{-1}\text{mol}^{-1}$ identifying the gas constant and $F = 96485.338\ \text{C mol}^{-1}$ the Faraday's constant. Furthermore, T denotes temperature, k_{f_0} and k_{b_0} are positive constants, ζ is an amplification factor. When $\zeta = 0$, the influence of the electric potential vanishes. This new formulation is consistent with the usual mass action law, which is recovered when the potential equals the reference potential, here taken as zero. Note that the equilibrium constants K_{eq} in Eqs. (2) or (4) remain independent upon the electric potential, which thus influences the velocity of the two reactions but not their equilibrium state.

2.2. Mass balance

The characteristic feature of our formulation is that positive ions are the only moving species. Uncompensated negative charges do not possess any intrinsic motility, hence there is no flow $\vec{h}_{\text{n}}^{-}(x,t)$ of negative charges. The concentration of vacancies is altered merely by the chemical ionization reaction (3).

In view of Eq. (1), every lithium ion that leaves the host site creates a negatively charged uncompensated vacancy. Therefore, since the amorphous structure is not suppose to reorder itself, the concentration of the vacancies plus the concentration of immobile lithium shall remain constant in time and equal the maximal concentration of host-sites

$$c_{\text{Li}_0} + c_{\text{n}}^{-} = c_0\,. \tag{7}$$

The mass balance equations model the transport of species within the solid electrolyte. Continuity equations are stated in a general, three-dimensional framework, although applications in this note will be merely one-dimensional (see Section 6). For the immobile lithium Li_0 and for uncompensated negative charges n^-, the mass balance equations do not account for fluxes

$$\frac{\partial c_{\text{Li}_0}}{\partial t} = -w, \tag{8a}$$

$$\frac{\partial c_{\text{n}^-}}{\partial t} = w, \tag{8b}$$

where w emanates from the mass action law (6a). For the interstitial and hopping processes the mass balance equations read

$$\frac{\partial c_{\text{Li}^+}}{\partial t} + \text{div}\left[\vec{h}_{\text{Li}^+}\right] = w - y, \tag{9a}$$

$$\frac{\partial c_{\text{Li}^+_{\text{hop}}}}{\partial t} + \text{div}\left[\vec{h}_{\text{Li}^+_{\text{hop}}}\right] = y, \tag{9b}$$

where the reaction rate of the interstitial-hopping transformation y is recovered from Eq. (6b).

2.3. Charge balance

Charges in the solution are due to negatively charged uncompensated vacancies as well as to the transport of interstitial and hopping positive ions:

$$\zeta = F\left(c_{\text{Li}^+} + c_{\text{Li}^+_{\text{hop}}} - c_{\text{n}^-}\right). \tag{10a}$$

The flux of mass in balance (9) of each species contributes to a current density $\vec{i}$

$$\vec{i} = F\left(\vec{h}_{\text{Li}^+} + \vec{h}_{\text{Li}^+_{\text{hop}}}\right). \tag{10b}$$

2.4. Maxwell's equations for electro-quasi-statics

The model identified so far involves 4 different species, whose concentrations are c_{Li_0}, c_{n^-}, c_{Li^+}, and $c_{\text{Li}^+_{\text{hop}}}$. The set of 4 mass balance equations, (8) and (9), contains 5 unknowns, i.e. the 4 mass concentrations plus the electric potential, which is constitutively related to the mass fluxes. An additional equation is required and a common selection in battery modeling is the *electroneutrality* condition (see among others [26], page 286), which for the model at hand reads

$$c_{\text{Li}^+}(\vec{x},t) + c_{\text{Li}^+_{\text{hop}}}(\vec{x},t) = c_{\text{n}^-}(\vec{x},t)\,. \tag{11}$$

In several studies, originated by Newman [26] and collectively gathered in the terminology "porous electrode theory", condition (11) is used in place of Maxwell's law - see among others [18,27–35]. Taking advantage of Eq. (11), the electric field is not constrained in any way to satisfy Maxwell's equations. Remarkably, electroneutrality does violate[1] Maxwell's equations (see for instance [36]).

[1] This is immediately accomplished in 1D, where in view of electroneutrality Gauss law reads $\frac{\partial D}{\partial x} = 0$, thus leading to a constant electric field.

As discussed in [12,17], the electroneutrality assumption (11) cannot be used in multiscale approaches, since it does not ensure energy conservation in the scales transitions.[2] This is a major obstacle to the development of predictive theories for the battery response with multi-scale models [16,39–46].

In the batteries modeling literature [26,47,48], it is generally assumed that the electromagnetic fields and their interactions are *static*. This assumption implies vanishing interference effects between the electric and magnetic phenomena. As a consequence, the set of Maxwell's equations are replaced by their electrostatic counterparts, as for the steady current case [49]. In the present paper, Eq. (11) is not used as a fundamental law. Instead, electromagnetics is explicitly taken into account via the *electro-quasi-static* formulation [50] of Maxwell's equations,[3] following the same path of reasoning of [12]. By this approach, the time-dependent hyperbolic Maxwell's equations are replaced by parabolic equations that can be solved in a more simple way.

Gauss's laws relate the electric displacement and magnetic fields ($\vec{D}$ and $\vec{B}$ respectively) emanating from the distribution (10a) of electric charge ζ

$$\mathrm{div}\left[\vec{D}\right] = \zeta\,, \qquad \mathrm{div}\left[\vec{B}\right] = 0. \tag{12}$$

In the light of the simplification made, the time derivative of the magnetic field is negligible within Maxwell–Faraday's law of induction, hence the electric field is irrotational and derives from an *electrostatic potential* ϕ:

$$\vec{E} = -\nabla\left[\phi\right]. \tag{13}$$

Finally, Ampère's law (with Maxwell's correction)

$$\frac{\partial \vec{D}}{\partial t} + \vec{i} = \mathrm{curl}\left[\vec{H}\right] \tag{14}$$

relates the electrical current (10b) and the time variation of the electric displacement field to the *magnetizing field* $\vec{H}$. The impingement of the latter in Ampère's law cannot be disregarded in the simplified framework of electro-quasi-statics. Nonetheless, a differential form can be straightforwardly obtained from Ampère's law (14), after application of the divergence operator:

$$\mathrm{div}\left[\frac{\partial \vec{D}}{\partial t} + \vec{i}\right] = 0. \tag{15}$$

2.5. Weak form and boundary conditions

A weak form that entails a proper energy meaning can be given as in [12] multiplying the strong form of the mass balance equations by a suitable set of chemical potentials test functions ($\hat{\mu}_{\mathrm{Li}_0}$, $\hat{\mu}_{\mathrm{n}^-}$, $\hat{\mu}_{\mathrm{Li}^+}$, $\hat{\mu}_{\mathrm{Li}^+_{\mathrm{hop}}}$) and performing integration by parts, exploiting Green's formula with the aim of reducing the order of differentiation. The weak forms of the mass balance Eqs. (8), (9) read:

$$\int_V \hat{\mu}_{\mathrm{Li}_0}\,\frac{\partial c_{\mathrm{Li}_0}}{\partial t}\,\mathrm{d}V = -\int_V \hat{\mu}_{\mathrm{Li}_0}\,w\,\mathrm{d}V\,, \tag{16a}$$

$$\int_V \hat{\mu}_{\mathrm{n}^-}\,\frac{\partial c_{\mathrm{n}^-}}{\partial t}\,\mathrm{d}V = \int_V \hat{\mu}_{\mathrm{n}^-}\,w\,\mathrm{d}V\,, \tag{16b}$$

$$\int_V \hat{\mu}_{\mathrm{Li}^+}\,\frac{\partial c_{\mathrm{Li}^+}}{\partial t} - \nabla\left[\,\hat{\mu}_{\mathrm{Li}^+}\right]\cdot\vec{h}_{\mathrm{Li}^+}\,\mathrm{d}V + \int_{\partial V}\hat{\mu}_{\mathrm{Li}^+}\,\vec{h}_{\mathrm{Li}^+}\cdot\vec{n}\,\mathrm{d}\Gamma = \int_V \hat{\mu}_{\mathrm{Li}^+}\,(w-y)\,\mathrm{d}V\,, \tag{16c}$$

$$\int_V \hat{\mu}_{\mathrm{Li}^+_{\mathrm{hop}}}\,\frac{\partial c_{\mathrm{Li}^+_{\mathrm{hop}}}}{\partial t} - \nabla\left[\hat{\mu}_{\mathrm{Li}^+_{\mathrm{hop}}}\right]\cdot\vec{h}_{\mathrm{Li}^+_{\mathrm{hop}}}\,\mathrm{d}V + \int_{\partial V}\hat{\mu}_{\mathrm{Li}^+_{\mathrm{hop}}}\,\vec{h}_{\mathrm{Li}^+_{\mathrm{hop}}}\cdot\vec{n}\,\mathrm{d}\Gamma = \int_V \hat{\mu}_{\mathrm{Li}^+_{\mathrm{hop}}}\,y\,\mathrm{d}V\,, \tag{16d}$$

where $\vec{n}$ denotes the outward normal. The electrolyte boundary ∂V, which forms the interfaces with the two electrodes, is of great relevance in energy storage systems. A large amount of research has been devoted to modeling the electrical double layer at solid-state electrochemical interfaces [52]. The weak form (16) clearly points out the need of splitting the lithium flux at the boundary into two terms,

$$\vec{h}_{\mathrm{Li}^+}\cdot\vec{n} = -h^{BV}_{\mathrm{Li}^+} \qquad \vec{x}\in\partial^N V\,, \tag{17a}$$

$$\vec{h}_{\mathrm{Li}^+_{\mathrm{hop}}}\cdot\vec{n} = -h^{BV}_{\mathrm{Li}^+_{\mathrm{hop}}} \qquad \vec{x}\in\partial^N V\,, \tag{17b}$$

where the mass fluxes at the boundary, termed $h^{BV}_{\mathrm{Li}^+}$ and $h^{BV}_{\mathrm{Li}^+_{\mathrm{hop}}}$, must descend from a proper interface equation, generally of Butler–Volmer type. Discussions on the electrode kinetics are differed to Section 8.

With a similar path of reasoning and accounting for Eq. (10b), the weak form of Ampère's law (15) reads

$$\int_V -\nabla\left[\hat{\phi}\right]\cdot\left\{\frac{\partial\vec{D}}{\partial t} + F\left(\vec{h}_{\mathrm{Li}^+} + \vec{h}_{\mathrm{Li}^+_{\mathrm{hop}}}\right)\right\}\mathrm{d}V + \int_{\partial V}\hat{\phi}\left\{\frac{\partial\vec{D}}{\partial t} + F\left(\vec{h}_{\mathrm{Li}^+} + \vec{h}_{\mathrm{Li}^+_{\mathrm{hop}}}\right)\right\}\cdot\vec{n}\,\mathrm{d}\Gamma = 0\,. \tag{18}$$

Boundary conditions for the electric potential emanate from Ampère's law (14), accounting for constraints (17).

$$\left\{\frac{\partial\vec{D}}{\partial t} + F\left(\vec{h}_{\mathrm{Li}^+} + \vec{h}_{\mathrm{Li}^+_{\mathrm{hop}}}\right)\right\}\cdot\vec{n} = \mathrm{curl}\left[\vec{H}\right]\cdot\vec{n} \qquad \vec{x}\in\partial V. \tag{19}$$

In modeling a full battery cell, as in Section 8, it can be assumed that the curl of the magnetizing field is continuous across all interfaces when projected in the normal direction. Such a continuity condition cannot be rephrased when the electrolyte only is modeled. It will be assumed in such a case that $\vec{B}$ *along the boundary* can be estimated from the "steady current" theory (see [49], chapter 3). Ampère's law without Maxwell's correction describes the magnetic field generated by a steady current

$$\mathrm{curl}\left[\vec{H}\right]\cdot\vec{n} = -F\left(h^{BV}_{\mathrm{Li}^+} + h^{BV}_{\mathrm{Li}^+_{\mathrm{hop}}}\right) \qquad \vec{x}\in\partial^N V. \tag{20}$$

In view of (17) and (19), boundary conditions for the electric potential read:

$$\frac{\partial\vec{D}}{\partial t}\cdot\vec{n} = 0 \qquad \vec{x}\in\partial^N V\,. \tag{21}$$

Note once again that this condition *is not imposed* in full cells. Finally, in order to make the problem solvable, Dirichlet boundary conditions (usually homogeneous) for the potential need to be added.

In conclusion, the weak form of the *balance* equations can be written in terms of the potentials in time interval $\left[0, t_f\right]$ as

$$\text{Find } z\in\mathcal{V}^{[0,t_f]} \text{ such that} \quad \frac{\mathrm{d}}{\mathrm{d}t}b(\hat{y},z(t)) + a(\hat{y},z(t)) + c(\hat{y},z(t)) = f(\hat{y}) \quad \forall\hat{y}\in\mathcal{V} \tag{22}$$

where

$$b(\hat{y},z) = \int_V \hat{\mu}_{\mathrm{Li}_0}\,c_{\mathrm{Li}_0} + \hat{\mu}_{\mathrm{n}^-}\,c_{\mathrm{n}^-} + \hat{\mu}_{\mathrm{Li}^+}\,c_{\mathrm{Li}^+} + \hat{\mu}_{\mathrm{Li}^+_{\mathrm{hop}}}\,c_{\mathrm{Li}^+_{\mathrm{hop}}}\,\mathrm{d}V - \int_V \nabla\left[\hat{\phi}\right]\cdot\vec{D}\,\mathrm{d}V \tag{23a}$$

$$a(\hat{y},z(t)) = -\int_V \nabla\left[\,\hat{\mu}_{\mathrm{Li}^+}\right]\cdot\vec{h}_{\mathrm{Li}^+} + \nabla\left[\hat{\mu}_{\mathrm{Li}^+_{\mathrm{hop}}}\right]\cdot\vec{h}_{\mathrm{Li}^+_{\mathrm{hop}}}\,\mathrm{d}V + \int_V \nabla\left[\hat{\phi}\right]\cdot F\left(\vec{h}_{\mathrm{Li}^+} + \vec{h}_{\mathrm{Li}^+_{\mathrm{hop}}}\right)\mathrm{d}V \tag{23b}$$

[2] In fact, in a rigorous multi scale mathematical formulation – see [37,38] – the micro to macro scale transition requires that the same power is expended at the two scales, thus assuring that energy is neither artificially generated nor artificially dissipated across the scales. If electroneutrality is used in place of Maxwell's equations, recovering the energy description of the electromagnetic interactions is hardly possible.

[3] As insightfully noticed in [50] electrostatics is a particular case of the general Maxwell's equations but electro-quasi-statics is not, it is *an approximation*. Such an approximation is acceptable under some conditions, described in [51].

$$c\,(\hat{y}, z(t)) = \int_V \hat{\mu}_{\mathrm{Li}_0}\cdot w\,\mathrm{d}V - \int_V \hat{\mu}_{\mathrm{n}^-}\cdot w\,\mathrm{d}V - \int_V \hat{\mu}_{\mathrm{Li}^+}\cdot (w-y)\,\mathrm{d}V - \int_V \hat{\mu}_{\mathrm{Li}^+_{\mathrm{hop}}}\cdot y\,\mathrm{d}V \tag{23c}$$

$$f\,(\hat{y}) = -\int_{\partial^N V} \hat{\mu}_{\mathrm{Li}^+} h^{BV}_{\mathrm{Li}^+} + \hat{\mu}_{\mathrm{Li}^+_{\mathrm{hop}}} h^{BV}_{\mathrm{Li}^+_{\mathrm{hop}}} - F\hat{\phi}\left(h^{BV}_{\mathrm{Li}^+} + h^{BV}_{\mathrm{Li}^+_{\mathrm{hop}}}\right)\,\mathrm{d}\Gamma \tag{23d}$$

with $z = \{c_{\mathrm{Li}_0}, c_{\mathrm{n}^-}, c_{\mathrm{Li}^+}, c_{\mathrm{Li}^+_{\mathrm{hop}}}, \phi\}$, $y = \{\mu_{\mathrm{Li}_0}, \mu_{\mathrm{n}^-}, \mu_{\mathrm{Li}^+}, \mu_{\mathrm{Li}^+_{\mathrm{hop}}}, \phi\}$. Columns z and y collect the time-dependent unknown fields. Column $\hat{y}$ collects the steady-state test functions that correspond to the unknown fields in y. To computationally solve the (either weak or strong) problem, constitutive equations must be specified, which is the subject of Section 3. Ellipticity of operators, functional and numerical properties of the solution and of its approximation depend on the constitutive assumptions and on the choice of the correct functional spaces $\mathcal{V}^{[0,t_f]}, \mathcal{V}$, whose identification falls beyond the scope of the present paper.

2.6. Equilibrium solution

We will discriminate the equilibrium conditions, that occur at no current flowing in the electrolyte, from the steady-state conditions, in which processes simply become time-independent. Chemical equilibrium for reaction (1) implies

$$c^{\mathrm{eq}}_{\mathrm{Li}_0} = \frac{c^{\mathrm{eq}}_{\mathrm{Li}^+}}{c^{\mathrm{eq}}_{\mathrm{Li}^+} + K^{\mathrm{ion}}_{\mathrm{eq}}}\,c_0\,, \qquad c^{\mathrm{eq}}_{\mathrm{n}^-} = \frac{K^{\mathrm{ion}}_{\mathrm{eq}}}{c^{\mathrm{eq}}_{\mathrm{Li}^+} + K^{\mathrm{ion}}_{\mathrm{eq}}}\,c_0\,. \tag{24}$$

In view of reaction (3), part of the lithium is transformed into hopping. Hence,[4] *at equilibrium*,

$$c^{\mathrm{eq}}_{\mathrm{Li}^+} + c^{\mathrm{eq}}_{\mathrm{Li}^+_{\mathrm{hop}}} = c^{\mathrm{eq}}_{\mathrm{n}^-} \quad \rightarrow c^{\mathrm{eq}}_{\mathrm{Li}^+_{\mathrm{hop}}} = \frac{K^{\mathrm{ion}}_{\mathrm{eq}}}{c^{\mathrm{eq}}_{\mathrm{Li}^+} + K^{\mathrm{ion}}_{\mathrm{eq}}}\,c_0 - c^{\mathrm{eq}}_{\mathrm{Li}^+}\,. \tag{25}$$

Chemical equilibrium of reaction (3) yields

$$K^{\mathrm{hop}}_{\mathrm{eq}}\,c^{\mathrm{eq}}_{\mathrm{Li}^+} - \left(\frac{K^{\mathrm{ion}}_{\mathrm{eq}}}{K^{\mathrm{ion}}_{\mathrm{eq}} + c^{\mathrm{eq}}_{\mathrm{Li}^+}}\,c_0 - c^{\mathrm{eq}}_{\mathrm{Li}^+}\right) = 0\,, \tag{26}$$

to be solved for c_{Li^+}. It yields

$$c^{\mathrm{eq}}_{\mathrm{Li}^+} = \frac{K^{\mathrm{ion}}_{\mathrm{eq}}}{2}\left(\sqrt{1 + 4\,\frac{c_0}{K^{\mathrm{ion}}_{\mathrm{eq}}}\,\frac{1}{1+K^{\mathrm{hop}}_{\mathrm{eq}}}} - 1\right), \tag{27}$$

to be replaced in Eqs. (24)–(25). Three independent parameters, therefore, shape the equilibrium concentrations, namely c_0 and the two equilibrium constant of reactions (1) and (3). Whereas the former can be estimated with accuracy, experimental estimation of $K^{\mathrm{ion}}_{\mathrm{eq}}$ and $K^{\mathrm{hop}}_{\mathrm{eq}}$ is subject to considerable uncertainties. The three parameters are connected to the fraction of Li that resides in equilibrium in the mobile state, termed here δ as in [15], i.e.

$$c^{\mathrm{eq}}_{\mathrm{Li}_0} = (1-\delta)\,c_0, \quad c^{\mathrm{eq}}_{\mathrm{n}^-} = \delta\,c_0\,. \tag{28}$$

Comparing eqs. ((24)b), (27), and ((28)b), it holds

$$\delta = \frac{2}{1 + \sqrt{1 + 4\,\frac{c_0}{K^{\mathrm{ion}}_{\mathrm{eq}}}\,\frac{1}{1+K^{\mathrm{hop}}_{\mathrm{eq}}}}}\,. \tag{29}$$

Eq. (29) can be easily inverted to obtain $K^{\mathrm{hop}}_{\mathrm{eq}}$ as a function of δ and $K^{\mathrm{ion}}_{\mathrm{eq}}$

$$K^{\mathrm{hop}}_{\mathrm{eq}} = \frac{-c_0\delta^2 + (1-\delta)K^{\mathrm{ion}}_{\mathrm{eq}}}{(\delta-1)K^{\mathrm{ion}}_{\mathrm{eq}}}. \tag{30}$$

[4] Note that Eq. (25) holds because at equilibrium we assume that concentrations are uniform, thus Eq. (25) merely expresses a mass conservation. Of course, out of equilibrium, the very same equation may describe electroneutrality, a constraint that is not imposed a priori in the present note. This point will be discussed further later on in the paper.

Since the latter can assume only positive values, Eq. (30) limits the region of admissible pairs $\{\delta, K^{\mathrm{ion}}_{\mathrm{eq}}\}$. The *upper bound* for $K^{\mathrm{ion}}_{\mathrm{eq}}$ is

$$\overline{K}^{\mathrm{ion}}_{\mathrm{eq}} = \frac{\delta^2}{1-\delta}\,c_0\,, \tag{31}$$

which, by coincidence, is the equilibrium constant of reaction (1) defined in [15]. In fact, a vanishing value for the equilibrium constant $K^{\mathrm{hop}}_{\mathrm{eq}}$ corresponds to $\overline{K}^{\mathrm{ion}}_{\mathrm{eq}}$ in identity (29).

3. Constitutive theory

For the sake of limiting the length of this note, we do not indulge in details on the thermodynamic balance of energy and entropy, which can be derived from [24] and from Appendix in [17]. Constitutive theory moves from the Helmholtz free energy density ψ that describes the isothermal processes at hand. It is assumed to consist of two separate contributions:

$$\psi(c_\alpha, \vec{E}) = \psi_{diff}(c_\alpha) + \psi_{el}(\vec{E})\,,$$

with $\alpha = \mathrm{Li}^+, \mathrm{Li}^+_{\mathrm{hop}}$. The mass transport process is described by ψ_{diff}, adopting species concentrations c_α as the state variables. The contribution $\psi_{el}(\vec{E})$ models the electromagnetic interactions, in terms of the electric field $\vec{E}$. The processes are thermodynamically uncoupled.

The electric displacement field is related to the electric field constitutively. In linear media

$$\psi_{el}(\vec{E}) = -\frac{1}{2}\,\text{ɬ}\,\vec{E}\cdot\vec{E} \tag{32}$$

whence, by means of identity (13),

$$\vec{D} = -\frac{\partial\psi_{el}(\vec{E})}{\partial\vec{E}} = \text{ɬ}\,\vec{E} = -\text{ɬ}\,\nabla[\,\phi\,] \tag{33}$$

The permittivity $\text{ɬ} = \text{ɬ}_r\,\text{ɬ}_0$ quantifies a material's ability to transmit (or "permit") an electric field. Its value is $8.85\times10^{-12}\ \mathrm{C\,V^{-1}\,m^{-1}}$ in vacuum (denoted with ɬ_0) . The permittivity of a homogeneous material is usually given relative to that of vacuum, as a relative permittivity ɬ_r.

The free energy $\psi_{diff}(c_{\mathrm{Li}^+}, c_{\mathrm{Li}^+_{\mathrm{hop}}})$ in a mixture, and in turn the chemical potentials

$$\mu_\alpha = \frac{\partial\psi_{diff}(c_\alpha)}{\partial c_\alpha}\,, \qquad \alpha = \mathrm{Li}^+, \mathrm{Li}^+_{\mathrm{hop}} \tag{34}$$

depend on the composition of the mixture itself. For no reasons but simplicity, we assume *ideal* conditions, and thus neglect the chemical interactions between Li^+ and $\mathrm{Li}^+_{\mathrm{hop}}$. We are aware of how strong this assumption can be, and will consider more intricate Maxwell–Stefan free energies in future works. In order to satisfy thermodynamic consistency, see among others [24] and appendix A in [17], a linear dependence of the mass flux of species α on the gradient of the electrochemical potential is taken

$$\vec{h}_\alpha = -\boldsymbol{M}_\alpha\,\nabla\left[\,\overline{\mu}_\alpha\,\right] \tag{35a}$$

by means of a positive definite mobility tensor $\boldsymbol{M}_\alpha$, with the electrochemical potential $\overline{\mu}_\alpha$ defined as

$$\overline{\mu}_\alpha = \mu_\alpha + F\,z_\alpha\,\phi\,. \tag{35b}$$

In *diluted solutions far from saturation*, the isotropic linear choice

$$\boldsymbol{M}_\alpha(c_\alpha) = \text{ϧ}_\alpha\,c_\alpha\,1 \tag{35c}$$

is taken, implying that the pure phase $c_\alpha = 0$ has a vanishing mobility. The amount $\text{ϧ}_\alpha > 0$ is usually termed the *ion mobility*. This approach is generally named after Fick's diffusion and captures an underlying Brownian motion of species in a statistical sense.

An *ideal solution model* [53] provides the following free energy density for the continuum approximation of the mixing for dilute solutions far from saturation

$$\psi^{id}_{diff}(c_{\mathrm{Li}^+}, c_{\mathrm{Li}^+_{\mathrm{hop}}}) = \mu^0_{\mathrm{Li}^+}\,c_{\mathrm{Li}^+} + \mu^0_{\mathrm{Li}^+_{\mathrm{hop}}}\,c_{\mathrm{Li}^+_{\mathrm{hop}}} + RT\left(c_{\mathrm{Li}^+}\,\ln[c_{\mathrm{Li}^+}] + c_{\mathrm{Li}^+_{\mathrm{hop}}}\,\ln[c_{\mathrm{Li}^+_{\mathrm{hop}}}]\right). \tag{36}$$

R is the universal gas constant, μ_α^0 is a reference value of the chemical potential of diffusing species α. Applying (34), the chemical potential results in the form

$$\mu_\alpha = \mu_\alpha^0 + RT\,(1+\ln[c_\alpha]) \tag{37}$$

and Fick's law (35) takes the Nernst–Planck form

$$\vec{h}_\alpha = -\mathbb{\mu}_\alpha\, RT\, \nabla\left[c_\alpha\right] - z_\alpha\, F\, \mathbb{\mu}_\alpha\, c_\alpha\, \nabla[\phi]\,. \tag{38}$$

The *diffusivity* $\mathbb{D}_\alpha$ is defined by $\mathbb{D}_\alpha = \mathbb{\mu}_\alpha\, RT$ (this equation is sometimes termed after Nernst–Einstein).

The hopping mechanism is thermodynamically quite different from the interstitial motion, thus making recourse to the classical Nernst–Planck thermodynamic description for both mechanisms might be questionable. Nonetheless, such a form is generally accepted in the literature (see for instance [11,15,18,34]). Within this paper, we assume that the fluxes $\vec{h}_{\mathrm{Li}^+}$ and $\vec{h}_{\mathrm{Li}^+_{\mathrm{hop}}}$ in Eqs. (23) obey the Nernst–Planck Eq. (38).

Equilibrium conditions for the chemical reactions (1) and (3) can be achieved from thermodynamics, as well. They are detailed in Appendix.

4. Governing equations and their weak form

4.1. Multiscale compatible formulation

The unknown fields result from the thermodynamic choices made. They are concentrations c_{Li_0}, c_{n^-}, c_{Li^+}, $c_{\mathrm{Li}^+_{\mathrm{hop}}}$, and the electric potential ϕ. Governing equations at all points $\vec{x} \in V$ and times t come out incorporating the constitutive Eqs. (33) and (38) into the balance Eqs. (9) and (15). Besides Eq. (8), governing equations read:

$$\frac{\partial c_{\mathrm{Li}^+}}{\partial t} - \mathrm{div}\left[\mathbb{D}_{\mathrm{Li}^+}\,\nabla\left[c_{\mathrm{Li}^+}\right] + \frac{F\,\mathbb{D}_{\mathrm{Li}^+}}{RT}\,c_{\mathrm{Li}^+}\,\nabla[\phi]\right] = w - y \tag{39a}$$

$$\frac{\partial c_{\mathrm{Li}^+_{\mathrm{hop}}}}{\partial t} - \mathrm{div}\left[\mathbb{D}_{\mathrm{Li}^+_{\mathrm{hop}}}\,\nabla\left[c_{\mathrm{Li}^+_{\mathrm{hop}}}\right] + \frac{F\,\mathbb{D}_{\mathrm{Li}^+_{\mathrm{hop}}}}{RT}\,c_{\mathrm{Li}^+_{\mathrm{hop}}}\,\nabla[\phi]\right] = y \tag{39b}$$

$$\mathrm{div}\left[\mathbb{\phi}\,\nabla\left[\frac{\partial\phi}{\partial t}\right] + \frac{F^2}{RT}\left(\mathbb{D}_{\mathrm{Li}^+}\,c_{\mathrm{Li}^+} + \mathbb{D}_{\mathrm{Li}^+_{\mathrm{hop}}}\,c_{\mathrm{Li}^+_{\mathrm{hop}}}\right)\nabla[\phi]\right] +$$

$$\mathrm{div}\left[F\left(\mathbb{D}_{\mathrm{Li}^+}\nabla\left[c_{\mathrm{Li}^+}\right] + \mathbb{D}_{\mathrm{Li}^+_{\mathrm{hop}}}\,\nabla\left[c_{\mathrm{Li}^+_{\mathrm{hop}}}\right]\right)\right] = 0 \tag{39c}$$

together with mass action laws (6a), (6b).

It is typical in batteries to fully impose Neumann conditions for concentration, in terms of mass fluxes, during galvanostatic processes. Accordingly, conditions (17) and (21) are applied along Neumann boundaries $\partial^N V$. To ensure uniqueness, Dirichlet boundary conditions have to be imposed along part $\partial^D V$, being $\partial V = \partial^D V \cup \partial^N V$.

Initial conditions usually enforce equilibrium. They have been stated in Eqs. (24)–(27). Initial conditions for electric potential should match the boundary value problem at $t = 0$, and yield a uniform value at all $\vec{x} \in V$. At initial time, in fact, Gauss law (12) provides the necessary and sufficient equations to be solved for ϕ:

$$\mathrm{div}\left[-\mathbb{\phi}\,\nabla[\phi]\right] = F\left(c_{\mathrm{Li}^+} + c_{\mathrm{Li}^+_{\mathrm{hop}}} - c_{\mathrm{n}^-}\right) \qquad \vec{x} \in V,\ t = 0 \tag{40}$$

together with homogeneous boundary conditions for potential and current — in view of thermodynamic equilibrium at initial time.

The evolution problem can be formulated in a weak form as well. Following a Galerkin approach, weak forms are built *at a given time t* using "variations" of the same set of variables that rule the problem, namely concentrations $\hat{c}_\alpha$ and electric potential $\hat{\phi}$ which are solely depending upon the space variable $\vec{x}$. The weak form of the *governing* equations can thus be written in time interval $\left[0, t_f\right]$ as

Find $y \in \mathcal{V}^{[0,t_f]}$ such that

$$\frac{\mathrm{d}}{\mathrm{d}t}\,b\left(\hat{y}(\vec{x}), y(\vec{x},t)\right) + a(\hat{y}(\vec{x}), y(\vec{x},t)) + c(\hat{y}(\vec{x}), y(\vec{x},t)) = f(\hat{y}(\vec{x})) \qquad \forall \hat{y} \in \mathcal{V} \tag{41a}$$

where

$$b\,(\hat{y}, z) = \int_V \hat{c}_{\mathrm{Li}_0}\,c_{\mathrm{Li}_0} + \hat{c}_{\mathrm{n}^-}\,c_{\mathrm{n}^-} + \hat{c}_{\mathrm{Li}^+}\,c_{\mathrm{Li}^+} + \hat{c}_{\mathrm{Li}^+_{\mathrm{hop}}}\,c_{\mathrm{Li}^+_{\mathrm{hop}}}$$

$$+\mathbb{\phi}\,\nabla\left[\hat{\phi}\right]\cdot\nabla\left[\frac{\partial\phi}{\partial t}\right]\mathrm{d}V \tag{41b}$$

$$a\,(\hat{y}, z(t)) = \int_V \mathbb{D}_{\mathrm{Li}^+}\nabla\left[\hat{c}_{\mathrm{Li}^+}\right]\cdot\nabla\left[c_{\mathrm{Li}^+}\right] + \frac{F\mathbb{D}_{\mathrm{Li}^+}}{RT}c_{\mathrm{Li}^+}\nabla\left[\hat{c}_{\mathrm{Li}^+}\right]\cdot\nabla[\phi]\,\mathrm{d}V +$$

$$+\int_V \mathbb{D}_{\mathrm{Li}^+_{\mathrm{hop}}}\nabla\left[\hat{c}_{\mathrm{Li}^+_{\mathrm{hop}}}\right]\cdot\nabla\left[c_{\mathrm{Li}^+_{\mathrm{hop}}}\right] + \frac{F\mathbb{D}_{\mathrm{Li}^+_{\mathrm{hop}}}}{RT}\,c_{\mathrm{Li}^+_{\mathrm{hop}}}\nabla\left[\hat{c}_{\mathrm{Li}^+_{\mathrm{hop}}}\right]\cdot\nabla[\phi]\,\mathrm{d}V +$$

$$+\int_V F\,\nabla\left[\hat{\phi}\right]\cdot\left(\mathbb{D}_{\mathrm{Li}^+}\,\nabla\left[c_{\mathrm{Li}^+}\right] + \mathbb{D}_{\mathrm{Li}^+_{\mathrm{hop}}}\,\nabla\left[c_{\mathrm{Li}^+_{\mathrm{hop}}}\right]\right)\mathrm{d}V$$

$$+\int_V \frac{F^2}{RT}\left(\mathbb{D}_{\mathrm{Li}^+}\,c_{\mathrm{Li}^+} + \mathbb{D}_{\mathrm{Li}^+_{\mathrm{hop}}}\,c_{\mathrm{Li}^+_{\mathrm{hop}}}\right)\nabla\left[\hat{\phi}\right]\cdot\nabla[\phi]\;\mathrm{d}V \tag{41c}$$

$$c\,(\hat{y}, z(t)) = \int_V \hat{c}_{\mathrm{Li}_0}\cdot w - \hat{c}_{\mathrm{n}^-}\cdot w - \hat{c}_{\mathrm{Li}^+}\cdot(w-y) - \hat{c}_{\mathrm{Li}^+_{\mathrm{hop}}}\cdot y\,\mathrm{d}V \tag{41d}$$

$$f\,(\hat{y}) = -\int_{\partial^N V} \hat{c}_{\mathrm{Li}^+}h^{BV}_{\mathrm{Li}^+} + \hat{c}_{\mathrm{Li}^+_{\mathrm{hop}}}\,h^{BV}_{\mathrm{Li}^+_{\mathrm{hop}}} - F\hat{\phi}\left(h^{BV}_{\mathrm{Li}^+} + h^{BV}_{\mathrm{Li}^+_{\mathrm{hop}}}\right)\mathrm{d}\Gamma \tag{41e}$$

with $y(\vec{x},t) = \{c_{\mathrm{Li}_0}, c_{\mathrm{n}^-}, c_{\mathrm{Li}^+}, c_{\mathrm{Li}^+_{\mathrm{hop}}}, \phi\}$ and $\hat{y}(\vec{x}) = \{\hat{c}_{\mathrm{Li}_0}, \hat{c}_{\mathrm{n}^-}, \hat{c}_{\mathrm{Li}^+}, \hat{c}_{\mathrm{Li}^+_{\mathrm{hop}}}, \hat{\phi}\}$.

4.2. Approximated electroneutral formulation

The hypothesis of electroneutrality, namely Eq. (11), leads to a simpler formulation for the governing equations. They encompass Eq. (11) itself, Eq. (8), Eq. (39a) and a linear combination of the former with (39b), which eventually leads to:

$$\mathrm{div}\left[\mathbb{D}_{\mathrm{Li}^+}\,\nabla\left[c_{\mathrm{Li}^+}\right] + \mathbb{D}_{\mathrm{Li}^+_{\mathrm{hop}}}\,\nabla\left[c_{\mathrm{Li}^+_{\mathrm{hop}}}\right]\right.$$

$$\left. + \frac{F}{RT}\left(\mathbb{D}_{\mathrm{Li}^+}\,c_{\mathrm{Li}^+} + \mathbb{D}_{\mathrm{Li}^+_{\mathrm{hop}}}\,c_{\mathrm{Li}^+_{\mathrm{hop}}}\right)\nabla[\phi]\right] = 0 \tag{42}$$

5. Steady state solution

At the end of the transient behavior, the solid electrolyte response reaches a steady state, at which the fields c_{Li_0}, c_{n^-}, c_{Li^+}, $c_{\mathrm{Li}^+_{\mathrm{hop}}}$, and ϕ do not change further in time. Current flows in the electrolyte at a steady state, hence the system is not at equilibrium.

A closed form solution at steady state can be found for one-dimensional systems under the assumption of electroneutrality. We may start from Eq. (8). Since the left hand side must vanish, then $w = 0$, i.e. the ionization reaction (1) must be at equilibrium. Hence, conditions (24) hold, here copied and pasted for readability

$$c^{\mathrm{ss}}_{\mathrm{Li}_0} = \frac{c^{\mathrm{ss}}_{\mathrm{Li}^+}}{c^{\mathrm{ss}}_{\mathrm{Li}^+} + K^{\mathrm{ion}}_{\mathrm{eq}}}\,c_0\,, \qquad c^{\mathrm{ss}}_{\mathrm{n}^-} = \frac{K^{\mathrm{ion}}_{\mathrm{eq}}}{c^{\mathrm{ss}}_{\mathrm{Li}^+} + K^{\mathrm{ion}}_{\mathrm{eq}}}\,c_0\,, \tag{43}$$

with the apex "ss" that stands for steady state. Enforcing electroneutrality, Eq. (11) implies

$$c^{\mathrm{ss}}_{\mathrm{Li}^+_{\mathrm{hop}}} = \frac{K^{\mathrm{ion}}_{\mathrm{eq}}}{K^{\mathrm{ion}}_{\mathrm{eq}} + c^{\mathrm{ss}}_{\mathrm{Li}^+}}\,c_0 - c^{\mathrm{ss}}_{\mathrm{Li}^+}. \tag{44a}$$

We are thus left with two unknown fields $c^{\mathrm{ss}}_{\mathrm{Li}^+}$ and ϕ^{ss}. They can be found solving Eqs. (42) and (39b), i.e.

$$-\mathrm{div}\left[\nabla\left[c^{\mathrm{ss}}_{\mathrm{Li}^+_{\mathrm{hop}}}\right] + \frac{F}{RT}\,c^{\mathrm{ss}}_{\mathrm{Li}^+_{\mathrm{hop}}}\,\nabla\left[\phi^{\mathrm{ss}}\right]\right] = -\frac{y}{\mathbb{D}_{\mathrm{Li}^+}}, \tag{45a}$$

$$-\mathrm{div}\left[\nabla\left[\frac{K_{\mathrm{eq}}^{\mathrm{ion}}}{K_{\mathrm{eq}}^{\mathrm{ion}}+c_{\mathrm{Li}^+}^{\mathrm{ss}}}c_0\right]+\frac{F}{RT}\left(\frac{K_{\mathrm{eq}}^{\mathrm{ion}}}{K_{\mathrm{eq}}^{\mathrm{ion}}+c_{\mathrm{Li}^+}^{\mathrm{ss}}}c_0\right)\nabla\left[\phi^{\mathrm{ss}}\right]\right]$$

$$=\left(\frac{1}{\mathbb{D}_{\mathrm{Li}^+_{\mathrm{hop}}}}-\frac{1}{\mathbb{D}_{\mathrm{Li}^+}}\right)y, \tag{45b}$$

with y as in (6b). A uniform concentration $c_{\mathrm{Li}^+}^{\mathrm{ss}}(x)=\bar{c}_{\mathrm{Li}^+}$ is sought for. In this circumstance, summing up the two Eqs. (45a), (45b) and rearranging, the laplacian of the electric potential turns out to be defined through an unknown constant p as follows

$$\mathrm{div}\left[\nabla\left[\phi\right]\right]=\frac{1}{\mathbb{D}_{\mathrm{Li}^+}}\frac{k_f^{\mathrm{hop}}\,\bar{c}_{\mathrm{Li}^+}-k_b^{\mathrm{hop}}\left(\frac{K_{\mathrm{eq}}^{\mathrm{ion}}}{K_{\mathrm{eq}}^{\mathrm{ion}}+\bar{c}_{\mathrm{Li}^+}}c_0-\bar{c}_{\mathrm{Li}^+}\right)}{\frac{F}{RT}\left(\bar{c}_{\mathrm{Li}^+}-\frac{K_{\mathrm{eq}}^{\mathrm{ion}}}{K_{\mathrm{eq}}^{\mathrm{ion}}+\bar{c}_{\mathrm{Li}^+}}c_0\right)}=p\,e^{\frac{\zeta F\phi}{RT}}\,, \tag{46}$$

taking advantage of Eq. (6). Note that the numerator in Eq. (46) is equal to y from Eq. (6b). Restricting to a one-dimensional problem, the solution of (46) is

$$\phi=a+bx+\frac{R^2T^2}{\zeta^2F^2}\,p\,e^{\frac{\zeta F\phi}{RT}}\,.$$

Imposing $\phi(0)=0$ and the conservation of current $\vec{h}_{\mathrm{Li}^+}(L)+\vec{h}_{\mathrm{Li}^+_{\mathrm{hop}}}(L)=\vec{h}_{\mathrm{Li}^+}(0)+\vec{h}_{\mathrm{Li}^+_{\mathrm{hop}}}(0)$, the constant p must vanish. As a consequence, y must vanish, too, thus granting chemical equilibrium. We conclude that, at steady state, the concentration

$$c_{\mathrm{Li}^+}^{\mathrm{ss}}=c_{\mathrm{Li}^+}^{\mathrm{eq}}$$

as in Eq. (27) and the electric potential is linear

$$\phi=b\,x\,, \tag{47}$$

with constant b identified by the current $\vec{h}_{\mathrm{Li}^+}(L)+\vec{h}_{\mathrm{Li}^+_{\mathrm{hop}}}(L)$ that flows across the electrolyte. Since the equilibrium concentrations are uniform, Nernst–Planck constitutive Eq. (38) has vanishing diffusive contribution and reduces to a special form of Ohm's law, with conductivity that depends upon concentration. From Faraday's law (10b), it eventually descends

$$\vec{i}=-\frac{F^2}{RT}\left(\mathbb{D}_{\mathrm{Li}^+}c_{\mathrm{Li}^+}^{\mathrm{ss}}+\mathbb{D}_{\mathrm{Li}^+_{\mathrm{hop}}}c_{\mathrm{Li}^+_{\mathrm{hop}}}^{\mathrm{ss}}\right)\nabla\left[\phi\right]. \tag{48}$$

6. Numerical simulations of the electrolyte response

To validate the model described so far, the *one-dimensional* solid electrolyte case study of [15] will be analyzed. The response of the electrolyte, part of a commercial all-solid-state thin-film battery with storage capacity of 0.7 mAh, is simulated under galvanostatic conditions of charge, at a constant temperature of 25 °C and zero state of stress. The electrolyte has been experimentally tested in [15] at different $C-rates$. All the parameters shared with [15] have been taken from that paper.

The electrolyte is a layer of LiPON with thickness 3.62 μm. We take for the $\mathrm{Li}^+_{\mathrm{hop}}$ diffusivity the vacancy diffusivity provided in [15], i.e. $\mathbb{D}_{\mathrm{Li}^+_{\mathrm{hop}}}=5.69\times10^{-16}\ \mathrm{m^2s^{-1}}$, whereas the interstitial lithium diffusivity holds $\mathbb{D}_{\mathrm{Li}^+}=1.73\times10^{-16}\ \mathrm{m^2s^{-1}}$. The relative permittivity of LiPON is assumed in the range of $1-100$. The fraction of Li that resides in equilibrium in the mobile state, δ is taken as in [15], i.e. $\delta=0.64$.

A few test-cases have been run changing the reaction constants parameters.

In order to make initial and boundary conditions compatible with thermodynamic equilibrium at $t=0$, the current $I(t)$ is tuned in time as

$$I(t)=(1-e^{-t})\,I_{1C} \tag{49}$$

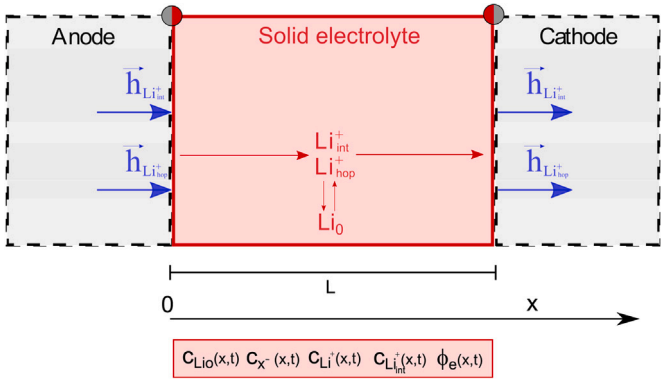

Fig. 2. A one-dimensional model of a Li-ion battery, with separator of size 3.62 μm highlighted. The flux of Li^+ ions during charge is pointed out.

with t in seconds and I_{1C} the current at 1C-rate, i.e. $I_{1C}=0.70$ mA. Boundary and initial conditions have been taken according to [15], adopting the coordinate system depicted in Fig. 2. Initially (at $t=0$) the concentration of ions across the electrolyte is uniform and at equilibrium as in Eqs. (24)–(27). The current passing through the electrode/electrolyte interfaces is the sum of the interstitial and hopping currents. Boundary conditions (17) thus shall satisfy the constraints

$$\left(\vec{h}_{\mathrm{Li}^+}(0,t)+\vec{h}_{\mathrm{Li}^+_{\mathrm{hop}}}(0,t)\right)\cdot\vec{n}=-\frac{I(t)}{FA}, \tag{50a}$$

$$\left(\vec{h}_{\mathrm{Li}^+}(L,t)+\vec{h}_{\mathrm{Li}^+_{\mathrm{hop}}}(L,t)\right)\cdot\vec{n}=\frac{I(t)}{FA}, \tag{50b}$$

where $A=3.36\times10^{-4}\ \mathrm{m^2}$ is the net area of the electrodes/electrolyte interfaces. For being in thermodynamic equilibrium with neither current nor mass flowing, the electric potential at the initial time satisfies Eqs. (40) and has to be homogeneous

$$\phi(x,0)=0\qquad\vec{x}\in V\,. \tag{51}$$

The boundary condition for ϕ at $x=0$ is homogeneous, too.

6.1. Discretization and time advancing by finite differences

The weak form (41) can be transformed in a first order Ordinary Differential Equation (ODE) in time if discretization is performed via separated variables, with spatial test $\varphi_i(x)$ and shape functions $\varphi_j(x)$ and nodal unknowns (collectively gathered in column y with component $y_j(t)$) that depend solely on time. The usual Einstein summation convention is taken henceforth for repeated indexes. The non linear ODE reads:

$$\text{Find } y(t) \text{ s.t.}\qquad b_i\cdot\frac{\partial y}{\partial t}(t)+a_i[\,y(t)\,]+c_i[\,y(t)\,]=f_i(t)$$
$$\text{for } i=1,2,\dots,N \tag{52a}$$

where

$$b_i\cdot\frac{\partial y}{\partial t}(t)=\int_0^l\varphi_i^{\mathrm{Li}_0}\varphi_j^{\mathrm{Li}_0}\,\mathrm{d}x\,\frac{\partial c_j^{\mathrm{Li}_0}}{\partial t}+\int_0^l\varphi_i^{\mathrm{n}^-}\varphi_j^{\mathrm{n}^-}\,\mathrm{d}x\,\frac{\partial c_j^{\mathrm{n}^-}}{\partial t}$$
$$+\int_0^l\varphi_i^{\mathrm{Li}^+}\varphi_j^{\mathrm{Li}^+}\,\mathrm{d}x\,\frac{\partial c_j^{\mathrm{Li}^+}}{\partial t}+ \tag{52b}$$

$$+\int_0^l\varphi_i^{\mathrm{Li}^+_{\mathrm{hop}}}\varphi_j^{\mathrm{Li}^+_{\mathrm{hop}}}\,\mathrm{d}x\,\frac{\partial c_j^{\mathrm{Li}^+_{\mathrm{hop}}}}{\partial t}+\int_0^l\notin\frac{\partial\varphi_i^{\phi}}{\partial x}\frac{\partial\varphi_j^{\phi}}{\partial x}\,\mathrm{d}x\,\frac{\partial\phi_j}{\partial t}$$

$$a_i[\,y(t)\,]=\int_0^l\mathbb{D}_{\mathrm{Li}^+}\frac{\partial\varphi_i^{\mathrm{Li}^+}}{\partial x}\frac{\partial\varphi_j^{\mathrm{Li}^+}}{\partial x}\,\mathrm{d}x\,c_j^{\mathrm{Li}^+}$$

Table 1
Model parameters used during simulations.

Input parameters			
Parameters	Value	Unit of measure	Description
T	298.5	°K	Temperature
L	$3.62 \cdot 10^{-6}$	m	Thickness of the electrolyte
A	$3.36 \cdot 10^{-4}$	m^2	Geometrical surface area
$\mathbb{D}_{Li^+}$	$5.69 \cdot 10^{-16}$	m^2/s	Diffusion coefficient for Li^+ ions in the electrolyte
$\mathbb{D}_{Li^+_{hop}}$	$1.73 \cdot 10^{-16}$	m^2/s	Diffusion coefficient for Li^+_{hop} in the electrolyte
δ	0.64	–	Fraction of mobile Li in the electrolyte in equilibrium
c_0	61141	mol/m^3	Maximal lithium concentration in the electrolyte

$$+\int_0^l \mathbb{D}_{Li^+_{hop}} \frac{\partial \varphi_i^{Li^+_{hop}}}{\partial x}\frac{\partial \varphi_j^{Li^+_{hop}}}{\partial x}\,dx\, c_j^{Li^+_{hop}} \tag{52c}$$

$$-F\int_0^l \frac{\partial \varphi_i^{\phi}}{\partial x}\mathbb{D}_{Li^+}\frac{\partial \varphi_j^{Li^+}}{\partial x}\,dx\, c_j^{Li^+}$$

$$-F\int_0^l \frac{\partial \varphi_i^{\phi}}{\partial x}\mathbb{D}_{Li^+_{hop}}\frac{\partial \varphi_k^{Li^+_{hop}}}{\partial x}\,dx\, c_k^{Li^+_{hop}} +$$

$$+\frac{F}{RT}\int_0^l \mathbb{D}_{Li^+}\frac{\partial \varphi_i^{Li^+}}{\partial x}\varphi_j^{Li^+}\frac{\partial \varphi_k^{\phi}}{\partial x}\,dx\, c_j^{Li^+}\phi_k +$$

$$+\frac{F}{RT}\int_0^l \mathbb{D}_{Li^+_{hop}}\frac{\partial \varphi_i^{Li^+_{hop}}}{\partial x}\varphi_j^{Li^+_{hop}}\frac{\partial \varphi_k^{\phi}}{\partial x}\,dx\, c_j^{Li^+_{hop}}\phi_k +$$

$$-\frac{F^2}{RT}\int_0^l \mathbb{D}_{Li^+}\frac{\partial \varphi_i^{\phi}}{\partial x}\frac{\partial \varphi_k^{\phi}}{\partial x}\varphi_j^{Li^+}\,dx\, c_j^{Li^+}\phi_k$$

$$-\frac{F^2}{RT}\int_0^l \mathbb{D}_{Li^+_{hop}}\frac{\partial \varphi_i^{\phi}}{\partial x}\frac{\partial \varphi_k^{\phi}}{\partial x}\varphi_j^{Li^+_{hop}}\,dx\, c_j^{Li^+_{hop}}\phi_k$$

$$\begin{aligned} c_i[\,y(t)\,] = &\int_0^l \varphi_i^{Li_0}\cdot(k_f^{ion}\varphi_j^{Li_0}c_j^{Li_0} - k_b^{ion}\varphi_j^{Li^+}c_j^{Li^+}\varphi_k^{n^-}c_k^{n^-})\,dx + \\ &-\int_0^l \varphi_i^{n^-}\cdot(k_f^{ion}\varphi_j^{Li_0}c_j^{Li_0} - k_b^{ion}\varphi_j^{Li^+}c_j^{Li^+}\varphi_k^{n^-}c_k^{n^-})dx \\ &-\int_0^l \varphi_i^{Li^+}\cdot\Big[(k_f^{ion}\varphi_j^{Li_0}c_j^{Li_0} - k_b^{ion}\varphi_j^{Li^+}c_j^{Li^+}\varphi_k^{n^-}c_k^{n^-}) + \\ &\qquad -(k_f^{hop}\varphi_j^{Li^+}c_j^{Li^+} - k_b^{hop}\varphi_j^{Li^+_{hop}}c_j^{Li^+_{hop}})\Big]\,dx + \\ &-\int_0^l \varphi_i^{Li^+_{hop}}\cdot(k_f^{hop}\varphi_j^{Li^+}c_j^{Li^+} - k_b^{hop}\varphi_j^{Li^+_{hop}}c_j^{Li^+_{hop}})\,dx \end{aligned} \tag{52d}$$

$$f_i(t) = \int_{\partial^N V}\varphi_i^{Li^+}h_{Li^+}^{BV} + \varphi_i^{Li^+_{hop}}h_{Li^+_{hop}}^{BV} - F\varphi_i^{\phi}\left(h_{Li^+}^{BV} + h_{Li^+_{hop}}^{BV}\right)\,d\Gamma \tag{52e}$$

with $y_j(t) = \{c_j^{Li_0}, c_j^{n^-}, c_j^{Li^+}, c_j^{Li^+_{hop}}, \phi_j\}$. A family of time-advancing methods based on the so-called θ-scheme can be set up for the discrete problem (52a). Assume that solution $y(t)$ is given at time t, and that the algorithm is triggered at the initial time $t = 0$ by means of initial conditions. The scheme seeks for $y(t + \Delta t)$ such that

$$\begin{aligned} b_i\cdot\frac{y(t+\Delta t)-y(t)}{\Delta t} &+ a_i[\,\theta\,y(t+\Delta t)+(1-\theta)y(t)\,] \\ &+ c_i[\,\theta\,y(t+\Delta t)+(1-\theta)y(t)\,] \\ &= \theta\,f_i(t+\Delta t)+(1-\theta)f_i(t) \end{aligned} \tag{53}$$

for $i = 1, 2, \ldots, N$, where $0 \le \theta \le 1$, $\Delta t = t_f/N_t$ is the time step, N_t is a positive integer. θ-scheme includes the forward Euler scheme ($\theta = 0$, linear in $y(t+\Delta t)$), backward Euler ($\theta = 1$), and Crank–Nicholson ($\theta = 1/2$). In the numerical simulations that follows, backward Euler ($\theta = 1$) has been selected, thus searching for $y(t + \Delta t)$ such that

$$b_i\cdot\frac{y(t+\Delta t)}{\Delta t} + a_i[\,y(t+\Delta t)\,] + c_i[\,y(t+\Delta t)\,] = f_i(t+\Delta t) + b_i\cdot\frac{y(t)}{\Delta t} \tag{54}$$

Denoting with $q = 1, 2, \ldots$ the iteration counter, the Newton Raphson iterative solution scheme solves non-linear problem (54). It proceeds until a condition on the L_2 norm of the increment

$$\delta y = {}^{q+1}y(t+\Delta t) - {}^{q}y(t+\Delta t)$$

is satisfied. The numerical technique has been implemented in a Matlab package script.

Several simulations have been carried out with different time steps and space discretizations in order to check convergence, but those details will not be presented here. The outcomes reported henceforth refer to a spatial discretization made of 20 finite elements, biased to a finer mesh in proximity of the boundaries, where greater gradient of the variables are expected. Time discretization is achieved with a constant time step $\Delta t = 1$ s.

Since the permittivity is extremely small, instabilities and convergence issue may arise. To this aim, the solution scheme has been partitioned into two separated algorithms. At first, the electroneutral approximation has been taken and the problem depicted in Section 4.2 has been solved. Such a solution is used as initial guess for the multiscale compatible formulation described in Section 4.1. Our strategy lacks of a profound numerical analysis investigation, yet neither stability nor convergence issues arose in the implementation of quasi electrostatic Maxwell's equation.

6.2. Steady state response

The closed form of steady state response of the system was established in Section 5. It is here computed numerically, using the material parameters collected in Table 1.

The concentrations $c_{Li_0}^{ss}$ and $c_{n^-}^{ss}$ emanate from Eq. (28), since chemical equilibrium is attained at the steady state. Easy algebra allows relating the steady state values for interstitial and hopping lithium to δ and K_{eq}^{ion}:

$$c_{Li^+}^{ss} = K_{eq}^{ion}\left(\frac{1}{\delta}-1\right), \quad c_{Li^+_{hop}}^{ss} = \delta\,c_0 + K_{eq}^{ion}\left(1-\frac{1}{\delta}\right). \tag{55}$$

Fig. 3 plots the evolution of $c_{Li^+}^{ss}$ and $c_{Li^+_{hop}}^{ss}$, normalized by the concentration of vacancies $c_{n^-}^{ss}$, at different values for K_{eq}^{ion} and δ. The red curve materializes the upper bound $\overline{K}_{eq}^{ion}$, defined in Eq. (31), corresponding to $K_{eq}^{hop} = 0$ in identity (30). Such a curve, in the $\{\delta, K_{eq}^{ion}\}$ plane, emerges at $c_{Li^+}^{ss} = c_{n^-}^{ss}$, as expected since no hopping takes place.

The molarity $c_{Li^+}^{ss}$ vanishes at $K_{eq}^{ion} = 0$: this outcome is expected, since no ions are generated in the chemical ionization reaction (1). On the other hand, as δ approaches the limit unit value, $c_{Li^+}^{ss}$ tends to zero again. In that case, the chemical ionization reaction (1) is complete, all host-sites became negative vacancies, K_{eq}^{hop} becomes larger and larger (see Eq. (30)). As a consequence, also reaction (3) becomes complete and no interstitial lithium is left over.

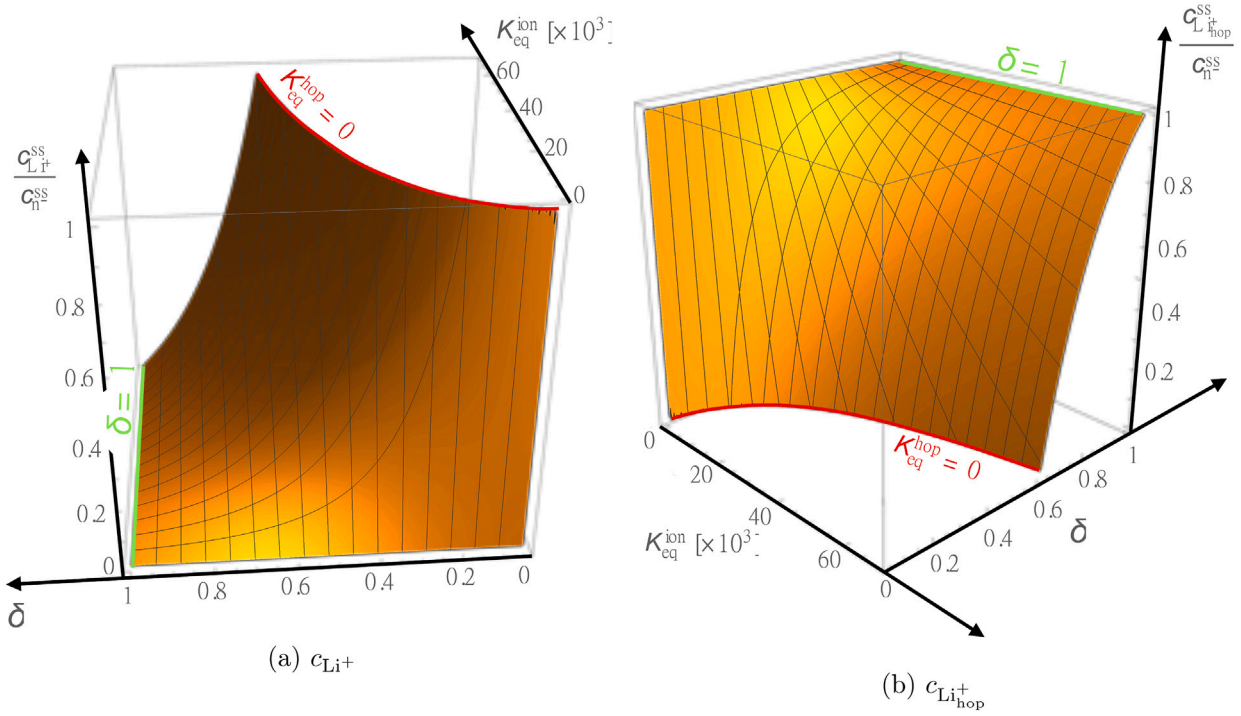

Fig. 3. Steady state representation of interstitial $c_{Li^+}^{ss}$ and hopping $c_{Li^+_{hop}}^{ss}$ lithium normalized by $c_{n^-}^{ss}$ as a function of δ and K_{eq}^{ion}. The red curve corresponds to the upper bound $\overline{K}_{eq}^{ion}$ defined in (31). (For interpretation of the references to color in this figure legend, the reader is referred to the web version of this article.)

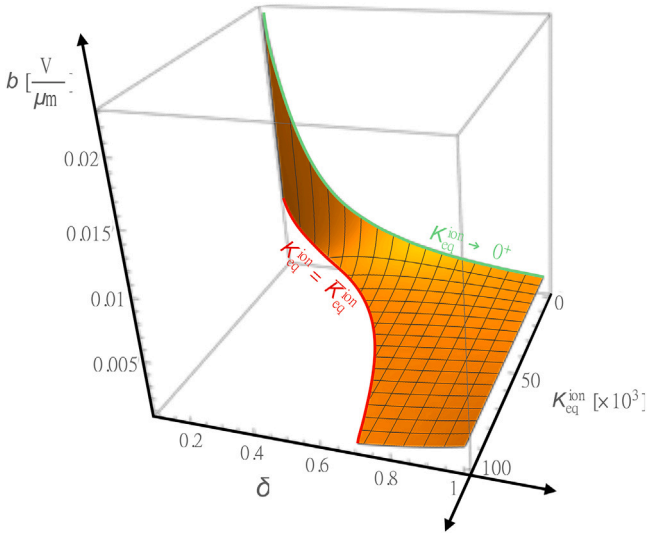

Fig. 4. Steady state representation of coefficient b (i.e. the gradient of the electric potential) as a function of δ and K_{eq}^{ion}. With the material properties of Table 1, $\underline{K}_{eq}^{ion} = 0$.

As per Eq. (47), the electric potential is linear. Coefficient b can be derived from Eq. (48) as

$$b = -\frac{I(t)}{A}\frac{RT}{F^2}\frac{1}{\mathfrak{D}_{Li^+}c_{Li^+}^{ss} + \mathfrak{D}_{Li^+_{hop}}c_{Li^+_{hop}}^{ss}}, \tag{56}$$

under the condition that the denominator is positive, i.e.

$$K_{eq}^{ion} > \overline{K}_{eq}^{ion}\frac{\mathfrak{D}_{Li^+_{hop}}}{\mathfrak{D}_{Li^+_{hop}} - \mathfrak{D}_{Li^+}}, \tag{57}$$

which in turn puts a condition on diffusivities in order to achieve a steady state condition, i.e.

$$\mathfrak{D}_{Li^+_{hop}} < \mathfrak{D}_{Li^+} \tag{58}$$

and sets $\underline{K}_{eq}^{ion} = 0$ as a *lower bound* on K_{eq}^{ion}. The values taken by b are plot in Fig. 4 as a function of δ and K_{eq}^{ion}.

The influence of the equilibrium constants K_{eq}^{ion} and K_{eq}^{hop} on the concentration of the species $c_{Li_0}^{ss}$, $c_{n^-}^{ss}$, $c_{Li^+}^{ss}$, $c_{Li^+_{hop}}^{ss}$ and on the gradient of the electric potential are shown in Figs. 5 and 6 for the particular value $\delta = 0.64$.

The steady state solution (28), (55) and (56) turns out to be the numerically simulated response of the electrolyte when initial conditions are imposed to be at equilibrium, according to Eqs. (24)–(27), and boundary conditions on fluxes (17) are chosen as such as to maintain such steady state solution.

6.3. Single discharge response of the electrolyte

The response of the system is studied at different values of material parameters.

6.3.1. Case study 1 : $K_{eq}^{ion} = \overline{K}_{eq}^{ion}$

The two reaction rate constants that describe the ionization reaction (1), i.e the lithium ion recombination rate k_b^{ion} and the generation rate k_f^{ion}, were identified in [15], $k_b^{ion} = 8.00 \cdot 10^{-7}$ m^{3}mol^{-1}s^{-1} and $k_f^{ion} = 5.56 \cdot 10^{-2}$ s^{-1}. Their ratio is $K_{eq}^{ion} = \overline{K}_{eq}^{ion} = 69518$ mol m^{-3}. As stated in Section 2.1, in such a case $K_{eq}^{hop} = 0$.

To follow the transient response of the electrolyte, analyses have been carried out perturbing the initial ionic concentration from the

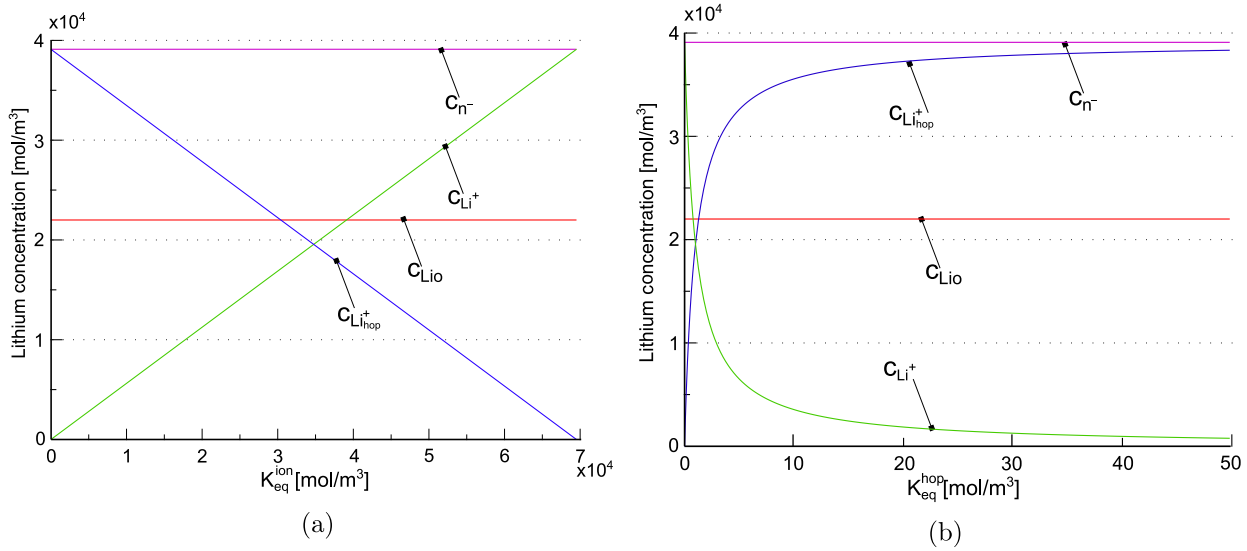

Fig. 5. Concentration of species $c^{ss}_{Li_0}$, $c^{ss}_{n^-}$, $c^{ss}_{Li^+}$, $c^{ss}_{Li^+_{hop}}$ as a function of K^{ion}_{eq} (a) and K^{hop}_{eq} (b) at $\delta = 0.64$ and $c_0 = 61141$.

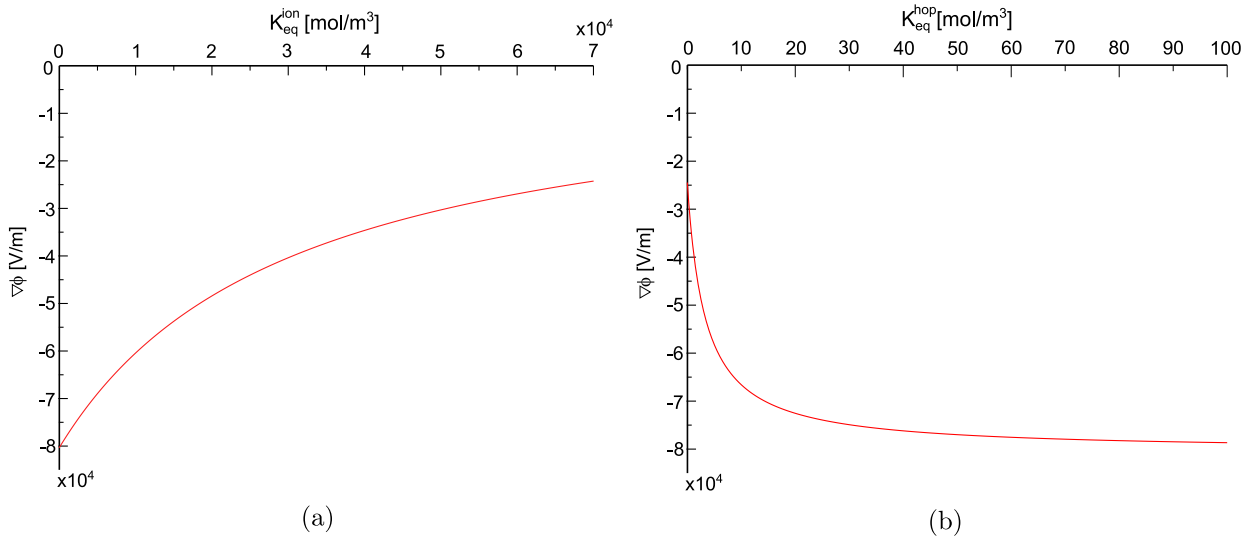

Fig. 6. Electric potential as a function of K^{ion}_{eq} (a) and K^{hop}_{eq} (b). The asymptotic values of the gradient of the electric potential are $b = -I(t)RT/(\delta AF^2 \mathfrak{P}_{Li^+_{hop}} c_0)$ for $K^{ion}_{eq} = 0$ and $b = -I(t)RT/(\delta AF^2 \mathfrak{P}_{Li^+} c_0)$ for $K^{ion}_{eq} = \overline{K}^{ion}_{eq}$.

state of equilibrium,[5] as follows:

$$c_{Li_0} = (1-\delta)c_0; \qquad c_{n^-} = \delta c_0; \qquad c_{Li^+} = 0.9 \cdot c_{n^-};$$
$$c_{Li^+_{hop}} = 0.1 \cdot c_{n^-} \qquad \vec{x} \in V,\ t = 0\,. \tag{59}$$

The initial concentration of hopping lithium will be transformed in interstitial by reaction (3), with pace ruled by the constant k_b^{hop}, with zero forward rate in view of this case-study hypothesis.

Consider first $k_b^{hop} = k_b^{ion}$. The transient evolution is clearly visible for species concentrations profiles at different instants (10, 30, 60 min, respectively) in Fig. 7. The oxygen-bound lithium concentration c_{Li_0} decreases in the whole electrolyte in the transient period, whereas vacancies do the opposite. Fig. 8, which focuses on the species concentrations at anode and cathode, shows that the concentration profiles acquire a steady state regime only after a very long time for the parameters at hand. One may argue therefore that, for some selections of parameters, the whole charge/discharge process occurs in the transient regime. The time required to approach a steady state regime is governed by the values of the reaction rate constants. Dotted lines in Fig. 8 denote the concentration of species at the interface with the anode, whereas continuous lines are used for the cathode interface.

Fig. 9a depicts the evolution of the electric potential $\phi(x)$ along the solid electrolyte at 10, 30, 60 min. It shows a tendency to reach the steady state much faster than concentrations. Fig. 9b reports the evolution of the electric potential at the cathode interface.

The deviation from perfect electroneutrality condition is estimated by the ratio ρ_{el}

$$\rho_{el}(t) = \sup_{0\le x\le L} \frac{c_{Li^+} + c_{Li^+_{hop}} - c_{n^-}}{c_{Li^+} + c_{Li^+_{hop}} + c_{n^-}}\,.$$

Electroneutrality is well approximated by the numerical solution, since $\rho_{el}(t) \sim 10^{-7}$ during the time-span of the discharge process.

To highlight the influence of k_b^{hop}, *we took* $k_b^{hop} = 1000 k_b^{ion}$ while keeping all other parameters unaltered. The increment of k_b^{hop} reduces

[5] If at the initial time $c_{Li^+_{hop}} = 0$ then no hopping lithium is further generated and no hopping takes place, with steady state charge transport of pure interstitial type.

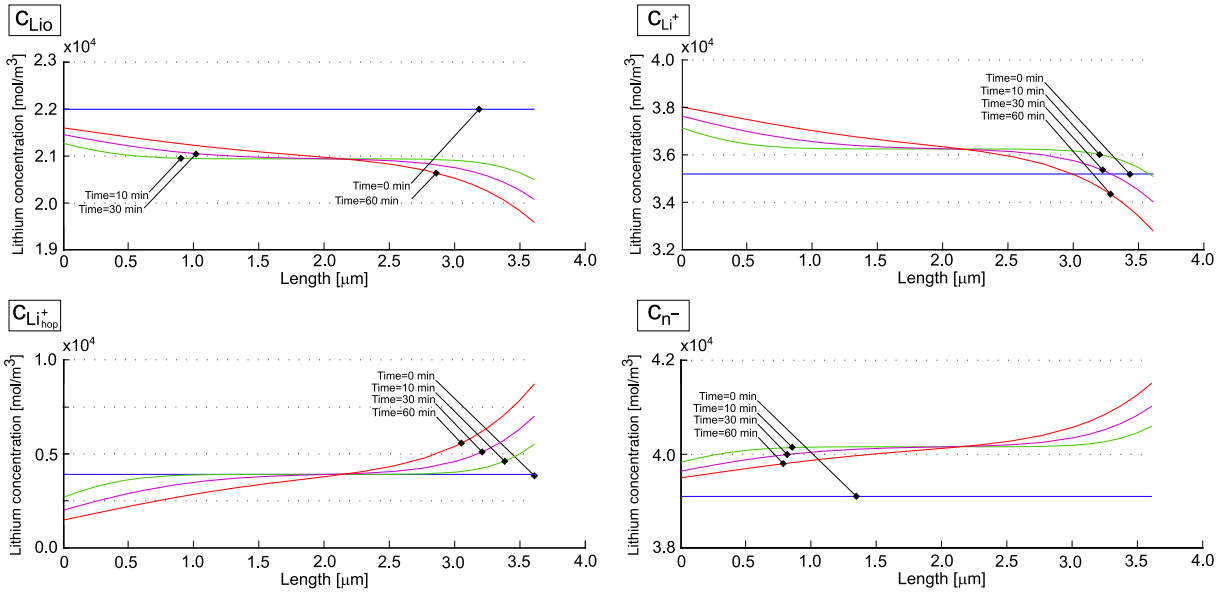

Fig. 7. Concentrations in the electrolyte. Four instants are considered: besides the initial time, 10 min, 30 min, 1 h.

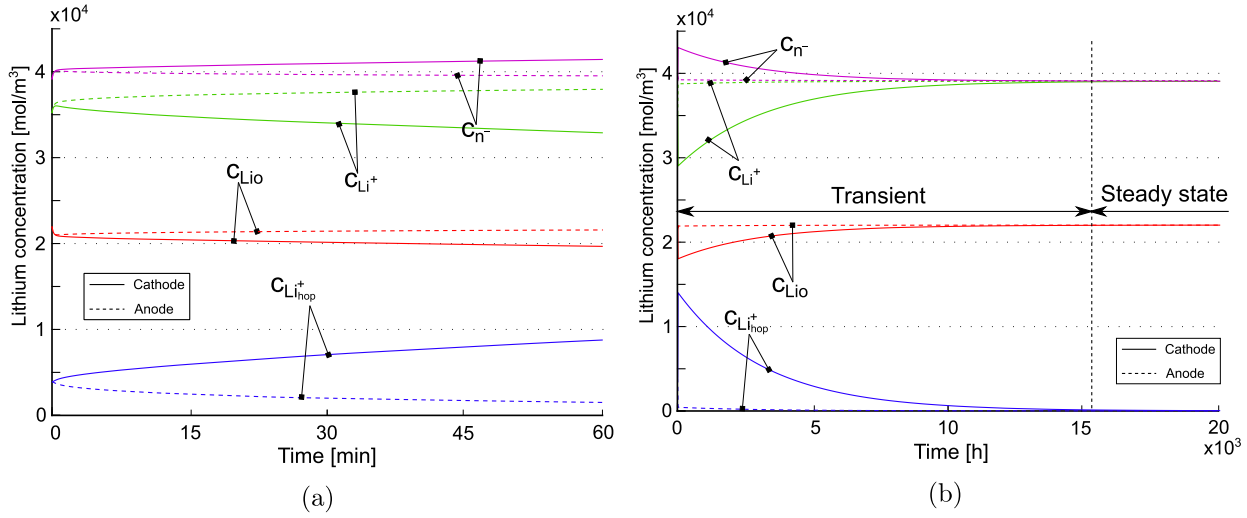

Fig. 8. Ionic concentration profile at anode and cathode for the different species. The dashed lines represent the values at the anode, the continuous lines at the cathode. (a) Zoom around $t = 0$ to show how concentration depart from initial values for the transient behavior. (b) A complete time-span evolution, showing how the steady asymptotic behavior is recovered.

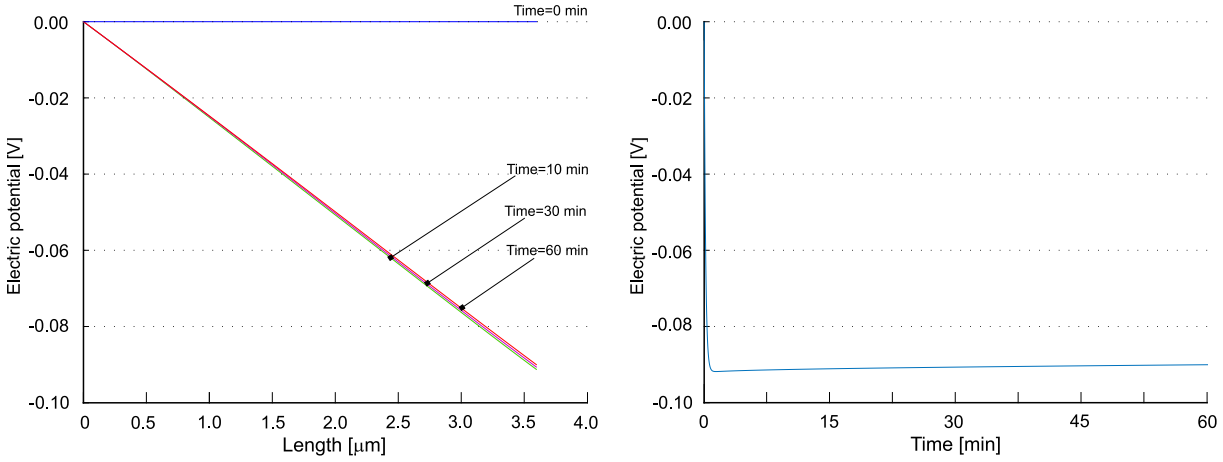

Fig. 9. (a) The electric potential $\phi(x)$, parametrized in time. (b) Its value $\phi(L)$ at the cathode interface.

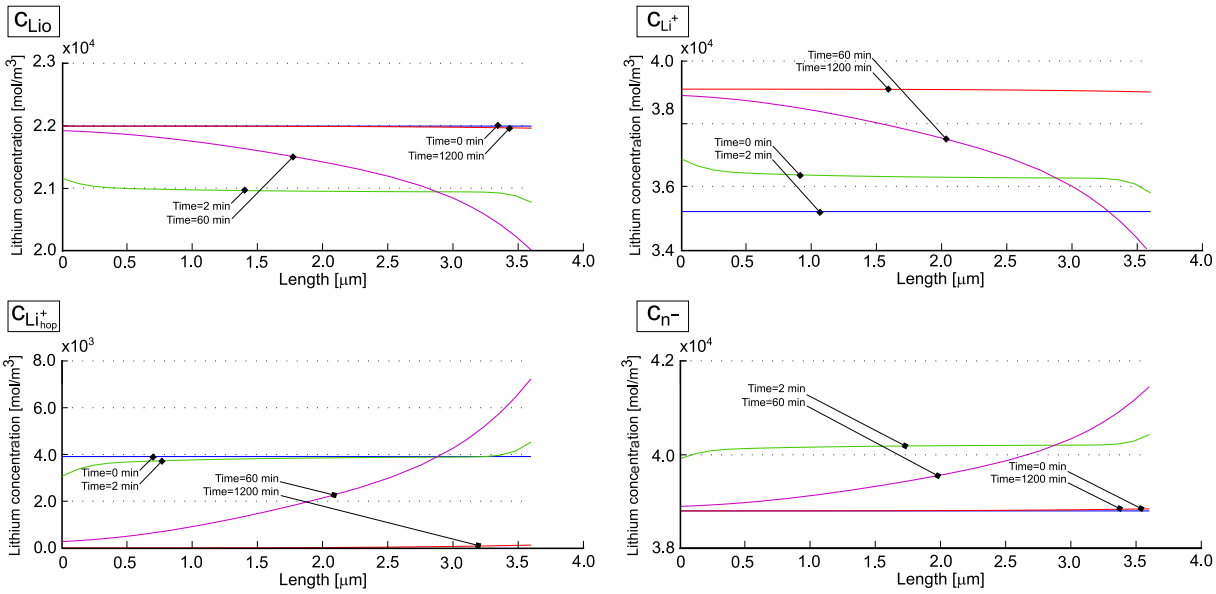

Fig. 10. Concentrations in the electrolyte. Four instants are considered, initial one (blue), 1 h (red), 10 min (green) and 30 min (yellow). $k_b^{\text{ion}} = 8.00 \cdot 10^{-7}$, $k_f^{\text{ion}} = 5.56 \cdot 10^{-2}$, $k_b^{\text{hop}} = 1000 k_b^{\text{ion}}$ and $k_f^{\text{hop}} = 0$. (For interpretation of the references to color in this figure legend, the reader is referred to the web version of this article.)

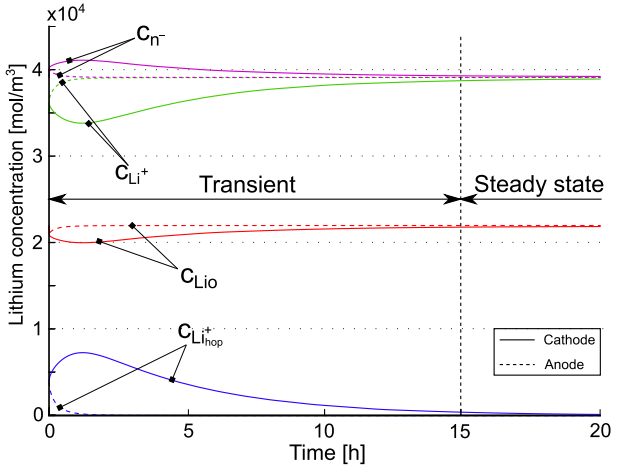

Fig. 11. Ionic concentration profile at the interface with the anode and the cathode. The dashed lines represent the values in the anode, the continuous lines in the cathode. $k_b^{\text{ion}} = 8.00 \cdot 10^{-7}$, $k_f^{\text{ion}} = 5.56 \cdot 10^{-2}$, $k_b^{\text{hop}} = 1000 k_b^{\text{ion}}$ and $k_f^{\text{hop}} = 0$.

significantly the time to reach the steady state regime, since the initial hopping lithium is much quickly converted into interstitial. Compare in this regard Fig. 11 with Fig. 8-b and Fig. 10a with Fig. 7.

6.3.2. *Case study 2 :* $K_{\text{eq}}^{\text{ion}} = 0.85\,\overline{K}_{\text{eq}}^{\text{ion}}$

In a second case study, the equilibrium constant $K_{\text{eq}}^{\text{ion}}$ has been reduced by fifteen percent, i.e. $K_{\text{eq}}^{\text{ion}} = 59090$ mol/m^3. The equilibrium constant for reaction (3) becomes $K_{\text{eq}}^{\text{hop}} = 0.1765$, from Eq. (29). The rate constant $k_b^{\text{ion}} = 8.00 \cdot 10^{-7}$ m^{3}mol^{-1}s^{-1} as in the previous case-study, and we consider $k_b^{\text{hop}} = k_b^{\text{ion}}$ at first. Initial conditions are taken as in (59).

The concentration of the different species in the electrolyte is plotted in Fig. 12. The overall response is similar to Fig. 7, but the steady state is reached more rapidly. Similar conclusion can be inferred from Fig. 13, where the concentrations at the two electrodes are shown.

As already noticed in the former case-study, the evolution of the electric potential $\phi(x)$ along the solid electrolyte shows a tendency to reach the steady state much faster than concentrations (see Fig. 14).

7. Sensitivity analysis of the model parameters

In this section we perform a Sensitivity Analysis (SA) to our model, in order to identify the importance of each parameter and its contribution to the variability of the model predictions derived in Section 6.2 at *steady state*. In ideal scenario, all the model parameters should be estimated as accurately as possible from carefully designed physical experiments. The cost and time restrictions, however, can limit the access to experimental data required for model calibration. Conducting a SA prior to the physical experiments can help in identifying the *essential* parameters (i.e. those with high *sensitivity index*) to be estimated. The *non-essential* parameters, on the other hand, can be set to nominal values obtained from the literature or any prior physical knowledge. Varying each parameter within a given range and scrutinizing the output of simulations allow identifying essential parameters.

Specifically, since Eq. (30) holds, three parameters are required to define the steady state solution, i.e. the maximal concentration of host-sites c_0, the fraction of Li that resides in equilibrium in the mobile state, δ, and the equilibrium constant of reaction (1), $K_{\text{eq}}^{\text{ion}}$. Assuming that c_0 can be estimated with high accuracy on theoretical grounds, the interest is to study the effect of δ and $K_{\text{eq}}^{\text{ion}}$ on the steady state solutions (55) and (56).

The Sobol' index, which is a variance-based method, is used to this aim. In the probabilistic setting, the model parameters are assumed to be random variables and a surrogate model is built to map the inputs to the corresponding output. Once the surrogate is constructed, Sobol decomposition provides the sensitivity indices [23]. We use the Bayesian Hybrid Modeling (GEBHM) approach [54,55], a probabilistic machine learning method that enables SA, calibration, multi-fidelity modeling and uncertainty quantification.

The matrix in Fig. 15(a) shows the correlation between the input parameters δ and $K_{\text{eq}}^{\text{ion}}$ and the output uniform concentrations $c_{\text{Li}^+}^{\text{ss}}$ and $c_{\text{Li}^+_{\text{hop}}}^{\text{ss}}$. We notice that δ has a small negative correlation with $c_{\text{Li}^+}^{\text{ss}}$ and relatively large positive correlation with $c_{\text{Li}^+_{\text{hop}}}^{\text{ss}}$. On the other hand, $K_{\text{eq}}^{\text{ion}}$ has a small negative correlation with $c_{\text{Li}^+_{\text{hop}}}^{\text{ss}}$ and positive correlation with $c_{\text{Li}^+}^{\text{ss}}$. This is expected given the structure of the expression relating the inputs to outputs (see Eq. (55)). Fig. 15(b) shows Sobol indices for the input parameters δ and $K_{\text{eq}}^{\text{ion}}$ representing the percentage of their contribution to the total variance of the outputs $c_{\text{Li}^+}^{\text{ss}}$ and $c_{\text{Li}^+_{\text{hop}}}^{\text{ss}}$,

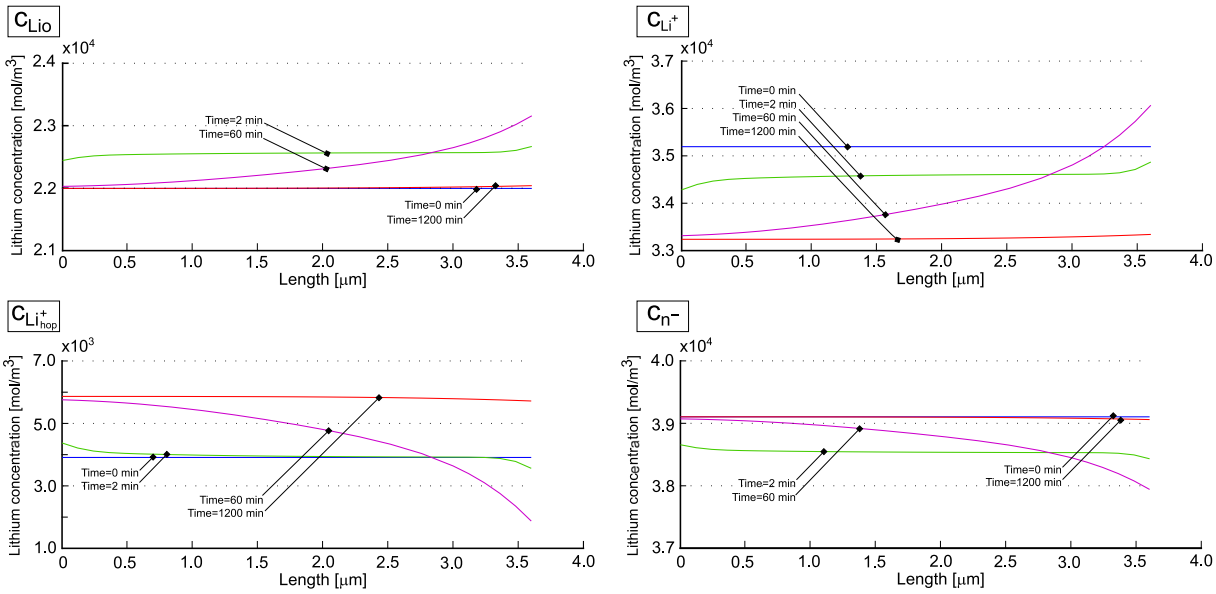

Fig. 12. Concentrations in the electrolyte. Four instants are considered, initial one (blue), 1 h (red), 10 min (green) and 30 min (yellow). $k_b^{\text{ion}} = 8.00 \cdot 10^{-7}$, $k_f^{\text{ion}} = 4.726 \cdot 10^{-2}$, $k_b^{\text{hop}} = 1000 k_b^{\text{ion}}$ and $k_f^{\text{hop}} = 1.4118 \cdot 10^{-4}$. (For interpretation of the references to color in this figure legend, the reader is referred to the web version of this article.)

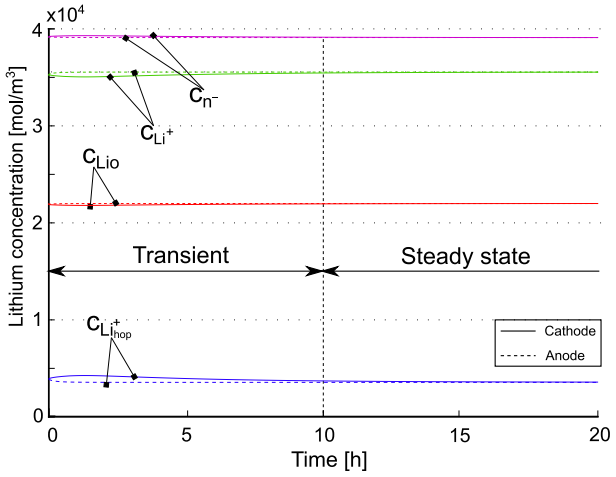

Fig. 13. Ionic concentration profile at the interface wit the anode and the cathode. The dashed lines represent the values in the anode, the continuous lines in the cathode. $k_b^{\text{ion}} = 8.00 \cdot 10^{-7}$, $k_f^{\text{ion}} = 4.726 \cdot 10^{-2}$, $k_b^{\text{hop}} = 1000 k_b^{\text{ion}}$ and $k_f^{\text{hop}} = 1.4118 \cdot 10^{-4}$.

respectively. The values of the total Sobol indices can be viewed as an indicator of the relevance of each parameter. For example in Fig. 15(b), δ contributes around 37% to the variability of $c^{\text{ss}}_{\text{Li}^+}$, whereas the interaction between δ and $K^{\text{ion}}_{\text{eq}}$ contributes around 48%. Similarly, Fig. 15(c) shows that δ contributes around 49% to the variability of $c^{\text{ss}}_{\text{Li}^+_{\text{hop}}}$. These results show that for the concentration $c^{\text{ss}}_{\text{Li}^+_{\text{hop}}}$, δ is the most influential parameter, while the interaction between δ and $K^{\text{ion}}_{\text{eq}}$ is the most influential on the variability of $c^{\text{ss}}_{\text{Li}^+}$. In conclusion, *the δ parameter should be carefully estimated prior to conducting any simulation*.

Next, we study in Fig. 16 the effect of the input parameters δ, $K^{\text{ion}}_{\text{eq}}$, $\mathbb{D}_{\text{Li}^+_{\text{hop}}}$, and $\mathbb{D}_{\text{Li}^+}$ on the variability of the coefficient b in Eq. (56). Once again majority of the variability is due to the variability in δ. The variability of the parameter $K^{\text{ion}}_{\text{eq}}$ alone has more effect than the individual variability of each $\mathbb{D}_{\text{Li}^+_{\text{hop}}}$, and $\mathbb{D}_{\text{Li}^+}$, while the interaction between δ with each $\mathbb{D}_{\text{Li}^+_{\text{hop}}}$ and $K^{\text{ion}}_{\text{eq}}$ comes in the third place. These results suggest again that *δ is the most sensitive parameter, even to the electric potential coefficient b.*

8. Numerical simulations of the electrolyte embodied in a full cell

In this section, the novel model of solid electrolyte illustrated so far is embodied in a thin film battery, with all-solid-state LiPON electrolyte. The full cell is eventually validated against the experimental outcomes described in [18].

The schematic representation of the battery under discharge conditions is shown in Fig. 17. The battery consists of a current collector, onto which the positive $LiCoO_2$ electrode is deposited, of a metallic lithium Li foil as negative electrode and of a LiPON solid-state electrolyte. One-dimensional mathematical models are customary formulations for thin films batteries, because: (i) the ratio between the lateral dimension and the thickness is large enough for the lateral dimension to be considered as infinite; (ii) thin electrodes and electrolyte are well approximated by homogeneous planar materials. The values of material and geometrical parameters are collected in Table 2.

During charge, the lithium ions cross the electrolyte and are reduced into metallic Li at the lithium foil surface; vice-versa during discharge. Assuming $LiCoO_2$ (shortened in LCO) to be the positive electrode material, the basic electrochemical charge-transfer reaction writes

$$\text{LiCoO}_2 \underset{k_{-1}}{\overset{k_1}{\rightleftarrows}} \text{Li}_{1-x}\text{CoO}_2 + x\text{Li}^+ + xe^- \quad 0 \le x \le \frac{1}{2}\,. \tag{60}$$

If lithium foil serves as the negative electrode material, deposition and extraction at the negative surface is described by the reaction

$$\text{Li} \underset{k_{-2}}{\overset{k_2}{\rightleftarrows}} \text{Li}^+ + e^-\,. \tag{61}$$

Li ions intercalating in the cathode will be denoted with $\text{Li}^{\oplus}$, to stress their ionic nature "shielded" by electrons and to distinguish them from mobile charges Li^+ in the electrolyte. Charge-transfer kinetics at both electrode/electrolyte interfaces, diffusion and migration of mobile lithium ions in the electrolyte (Li^+) and positive electrode ($\text{Li}^{\oplus}$) are accounted for. The space-charge separation in electrical double layers, materialized at both electrode/electrolyte interfaces, is considered, too. Redox processes, modeled as isothermal, only occur at the interfaces between the electrolyte and the electrode layers; volume changes of the electrolyte during cycling are neglected and the active surface area does not change over cycling.

The positive and negative electrodes thickness amount at $L_c = 0.32$ μm and $L_a = 0.50$ μm, respectively. The solid electrolyte is a one-micron-thick ($L_e = 1.00$ μm) layer of LiPON. The surface area of the

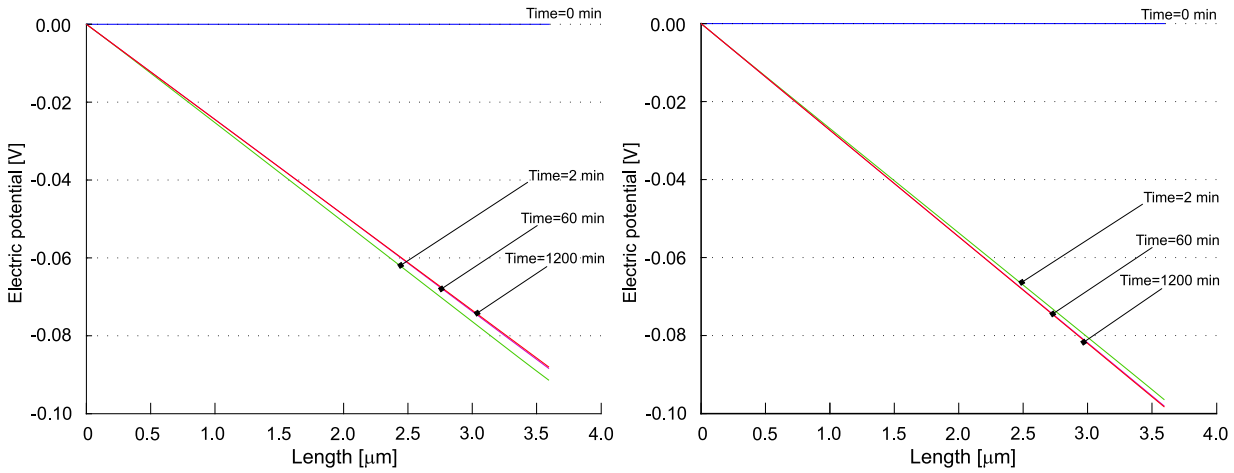

Fig. 14. The electric potential $\phi(x)$ inside the electrolyte. (a) $k_b^{\text{ion}} = 8.00 \cdot 10^{-7}$, $k_f^{\text{ion}} = 5.56 \cdot 10^{-2}$, $k_b^{\text{hop}} = 1000 k_b^{\text{ion}}$ and $k_f^{\text{hop}} = 0$. (b) $k_b^{\text{ion}} = 8.00 \cdot 10^{-7}$, $k_f^{\text{ion}} = 4.726 \cdot 10^{-2}$, $k_b^{\text{hop}} = 1000 k_b^{\text{ion}}$ and $k_f^{\text{hop}} = 1.4118 \cdot 10^{-4}$.

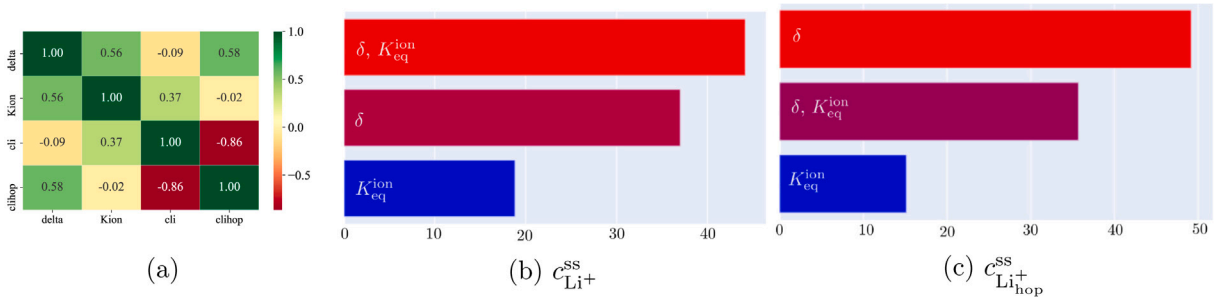

Fig. 15. The correlation matrix between the input and output (a). The total Sobol indices for: (b) $c_{\text{Li}^+}^{\text{ss}}$ and (c) $c_{\text{Li}_{\text{hop}}^+}^{\text{ss}}$.

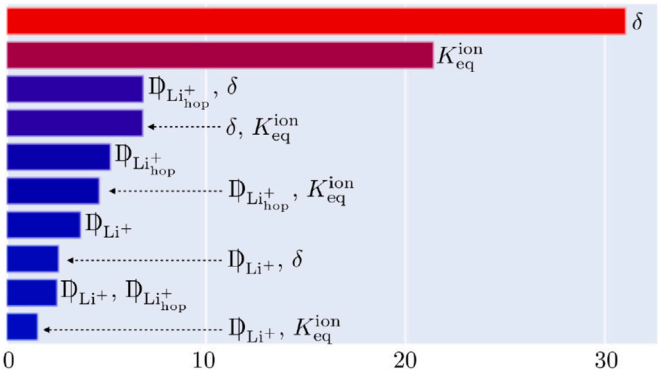

Fig. 16. The total Sobol indices for b.

deposited electrodes is $A = 10^{-4}$ m^2 and the theoretical storage capacity of the battery is 10^{-5} Ah.

The electrochemical cell is subject to a galvanostatic process of discharge at different $C-rates$, under a temperature-controlled condition of 25 °C. The current corresponding to $C-rate = j$ is denoted with I_{jC}. For $C-rate = 1$, I_{1C} amounts at $10^{-5} A$. Initial and boundary conditions are made compatible with thermodynamic equilibrium at $t = 0$, tuning the density current $i_{bat}(t)$ in time as:

$$i_{bat}(t) = (1 - e^{-t}) \frac{I_{jC}}{A}, \tag{62}$$

with t in seconds. In view of (62), all ionic concentrations at $t = 0$ are uniform and at equilibrium, because no profiles have yet developed. By enforcing the fraction of mobile lithium in the electrolyte $\delta = 0.18$ and a maximum concentration of lithium host sites in the electrolyte $c_0 = 60100\,\text{mol/m}^3$, Eqs. (24)–(28) provides

$$c_{\text{Li}}(x,0) = c_{\text{Li}}^{\text{eq}} = 2.40 \cdot 10^4 \quad \text{mol/m}^3 \quad -L_a \le x \le 0, \tag{63a}$$

$$c_{\text{Li}_0}(x,0) = 4.93 \cdot 10^4 \quad \text{mol/m}^3 \quad 0 \le x \le L_e, \tag{63b}$$

$$c_{\text{n}^-}(x,0) = 1.08 \cdot 10^4 \quad \text{mol/m}^3 \quad 0 \le x \le L_e, \tag{63c}$$

$$c_{\text{Li}^+}(x,0) = 5.68 \cdot 10^3 \quad \text{mol/m}^3 \quad 0 \le x \le L_e, \tag{63d}$$

$$c_{\text{Li}_{\text{hop}}^+}(x,0) = 5.12 \cdot 10^3 \quad \text{mol/m}^3 \quad 0 \le x \le L_e, \tag{63e}$$

$$c_{\text{Li}^\oplus}(x,0) = c_{\text{Li}^\oplus}^{\text{eq}} = 1.20 \cdot 10^4 \quad \text{mol/m}^3 \quad L_e \le x \le L_e + L_c. \tag{63f}$$

The electric potential at the interface between the anode and the solid electrolyte is fixed as:

$$\phi(0,t) = 0\ [V] \quad \forall t. \tag{64}$$

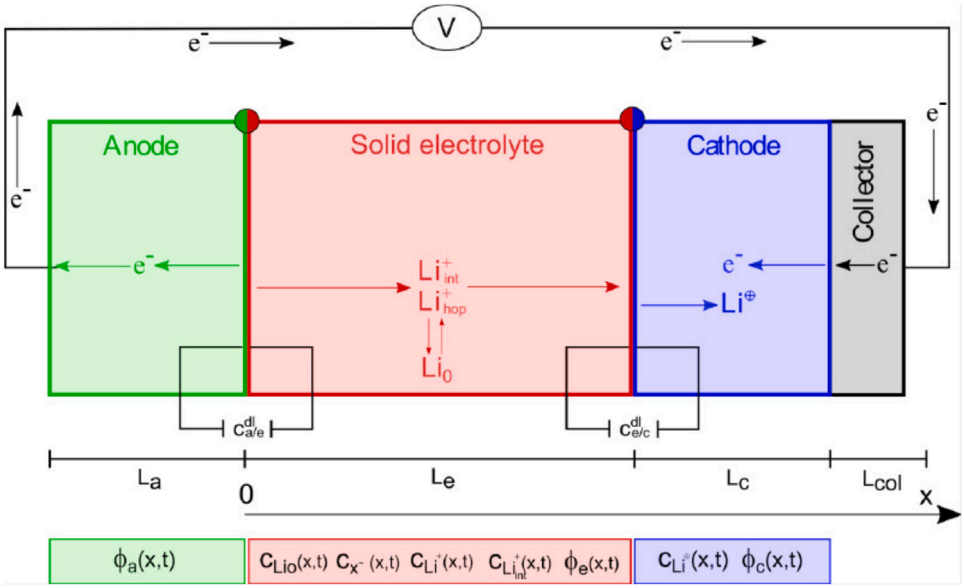

Fig. 17. A pictorial view of the ASSBs used to validate the solid electrolyte model proposed, under discharge conditions, together with the unknown fields. The unknown fields include lithium concentration in the anode, for the sake of generality.

Table 2
Model parameters used during simulations.

Input parameters			
Parameter	Value	Unit	Description
T	298.5	K	Temperature
L_a	$0.50 \cdot 10^{-6}$	m	Thickness of the anode
L_e	$1.50 \cdot 10^{-6}$	m	Thickness of the electrolyte
L_c	$0.32 \cdot 10^{-6}$	m	Thickness of the cathode
L_{col}	$0.10 \cdot 10^{-6}$	m	Thickness of the positive collector
A	$1.00 \cdot 10^{-4}$	m^2	Geometrical surface area
$c^{sat}_{Li^{\oplus}}$	$2.34 \cdot 10^{4}$	mol m^{-3}	Maximum concentration of $Li^{\oplus}$ ions in the electrode
k_a	$1.08 \cdot 10^{7}$	S m^{-1}	Electrical conductivities in the lithium anode
k_{col}	10.0	S m^{-1}	Electrical conductivities in the current collector
k^{ion}_f	$1.125 \cdot 10^{-5}$ ($1.80 \cdot 10^{-5}$)	s^{-1}	Lithium ion generation reaction rate constant for Eq. (1)
k^{ion}_b	$0.90 \cdot 10^{-8}$	m^3 mol^{-1} s^{-1}	Lithium ion recombination reaction rate constant for Eq. (1)
k^{hop}_f	$8.10 \cdot 10^{-9}$ ($1.69 \cdot 10^{-9}$)	s^{-1}	Lithium ion generation reaction rate constant for Eq. (3)
k^{hop}_b	$0.90 \cdot 10^{-8}$	m^3 mol^{-1} s^{-1}	Lithium ion recombination reaction rate constant for Eq. (3)
c^{dl}_a	$1.74 \cdot 10^{-4}$	F m^{-2}	Double layer capacity per unit area of anode
c^{dl}_c	$5.30 \cdot 10^{-3}$	F m^{-2}	Double layer capacity per unit area of cathode
α_n	0.6	–	Charge transfer coefficient for the negative electrode
α_p	0.6	–	Charge transfer coefficient for the positive electrode
$\mathfrak{D}_{Li^+}$	$5.10 \cdot 10^{-15}$	m^2 s^{-1}	Diffusion coefficient for Li^+ ions in the electrolyte
$\mathfrak{D}_{Li^+_{hop}}$	$0.90 \cdot 10^{-15}$	m^2 s^{-1}	Diffusion coefficient for Li^+_{hop} ions in the electrolyte
$\mathfrak{D}_{Li^{\oplus}}$	$1.76 \cdot 10^{-15}$	m^2 s^{-1}	Diffusion coefficient for $Li^{\oplus}$ ions in the cathode
k_1	$5.10 \cdot 10^{-6}$	$m^{2.5}$ $mol^{-0.5}$ s^{-1}	Standard reaction rate constant for forward reaction in Eq. (60)
k_2	$1.09 \cdot 10^{-5}$	m s^{-1}	Standard reaction rate constant for forward reaction in Eq. (61)
δ	0.18	–	Fraction of mobile ions in the electrolyte in equilibrium
c_0	$6.01 \cdot 10^{4}$	mol m^{-3}	Maximal lithium concentration in the electrolyte
ϵ_r	2.25	–	Relative permittivity in the electrolyte

According to Eqs. (2) and (4), the equilibrium constants read

$$K^{ion}_{eq} = \frac{1.125 \cdot 10^{-5}}{0.90 \cdot 10^{-8}} = 1250\,, \quad K^{hop}_{eq} = \frac{8.10 \cdot 10^{-9}}{0.90 \cdot 10^{-8}} = 0.9. \tag{65}$$

Solution schemes - The governing equations are numerically solved with the finite element method, with in house implementation of weak forms in the commercial numerical software Matlab. The geometry and the unknown fields (see Fig. 17) are discretized with 61 linear elements; 1 element is sufficient for the anode, since the lithium concentration is uniform ad the electric potential is linear; the outcomes refer to a tessellation of 40 finite elements covering the electrolyte and 20 panels that discretize the cathode. In both cases, the mesh is refined near the electrode/electrolyte interface. The time marching is dealt with the backward Euler method, with fixed time increments of $\Delta t = 1.0$ s.

The open circuit potential (OCP) used in the simulations has been reconstructed with splines stemming from experimental evidences in [18].

The simulations account for a broad range of C-rates, from 1.0 to 51.2. The corresponding experimental discharging curves have been plotted with dots in Fig. 18-a as a function of time: continuous lines correspond to simulations. Measurements and simulations agree well across the wide range of investigated $C-rates$. Obviously, the extracted charge decreases with increasing $C-rate$ due to the higher over-potentials. In fact lower discharge rates implies a lower rate of lithium insertion in the cathode and a more uniform Li distribution in the positive electrode.

Electric potential profiles - Fig. 19 depicts the electric potential $\phi(x)$ profile in the battery at different times for two different discharge

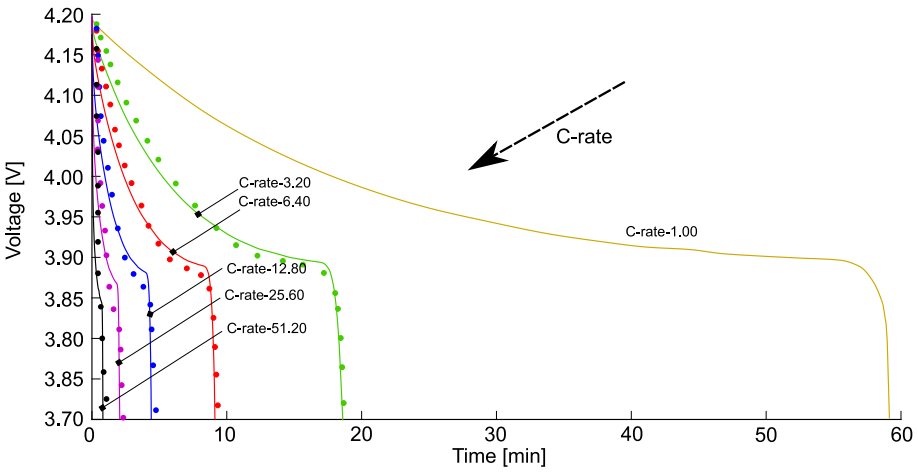

Fig. 18. Voltage vs time discharge curves as a function of time for different $C-rates$. Colored lines correspond to different $C-rates$, whereas the dots identify the experimental values. (For interpretation of the references to color in this figure legend, the reader is referred to the web version of this article.)

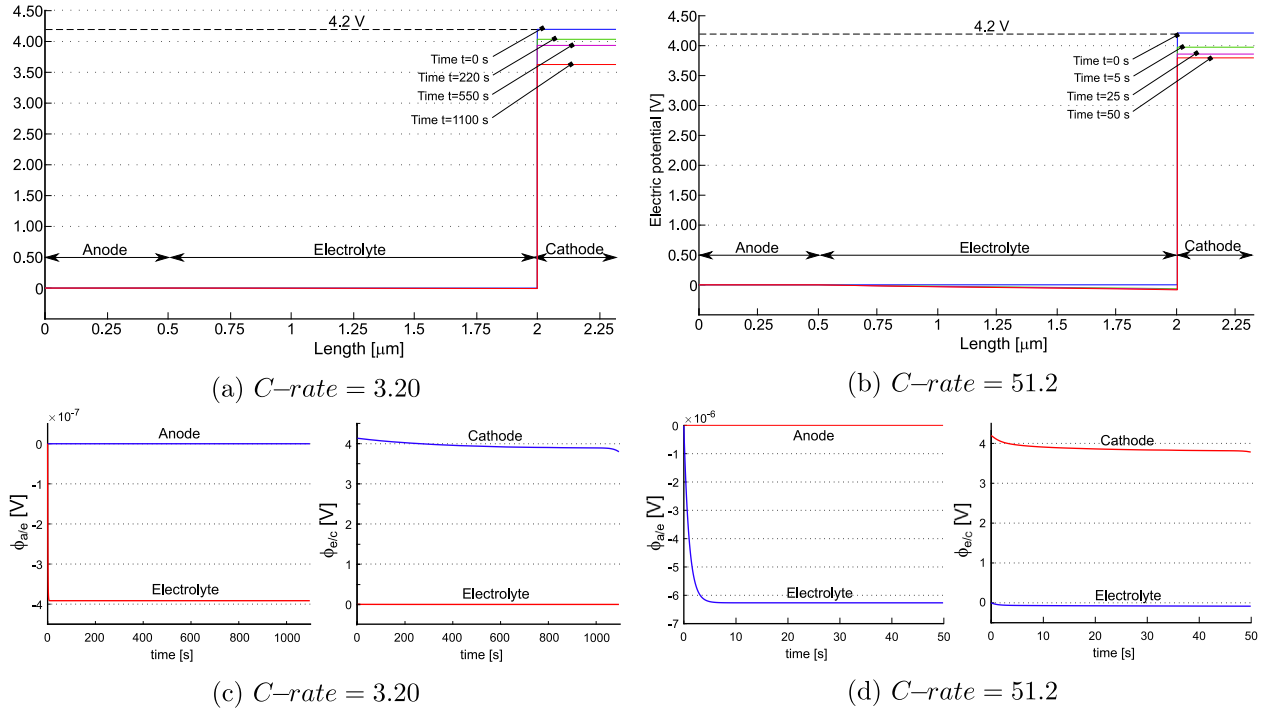

Fig. 19. (a)–(b): The electric potential profile at different times for two different $C-rates$. The last plotted time step corresponds to the instant when the concentration of lithium $Li^{\oplus}$ inside the cathode reaches the saturation limit $c^{sat}_{Li^{\oplus}}$. (c)–(d): The electric potential in the interfaces with the electrodes as a function of time for two different $C-rates$.

rates, i.e. $C-rate = 3.20$ (which theoretically allows to discharge the battery in 1125 s) and $C-rate = 51.2$ (for which the battery in principle completes the discharge process in 70 s). Simulations quit when the concentration of lithium $Li^{\oplus}$ inside the cathode reaches the saturation limit $c^{sat}_{Li^{\oplus}}$, after 1085 s and 50 s respectively. Cathodic saturation is indeed the limit factor for the battery operation (see also [56] for an extensive discussion on limiting factors in electrochemical cells, induced by materials and architectures).

The electric potential evolution in time at both interfaces is given in Fig. 19(c)–(d) and reflects the conclusions driven in Fig. 19(a)–(b).

Interface currents - Interface conditions on fluxes at the left and right boundaries of the electrolyte are:

$$\vec{h}_{Li^+}(0,t)\cdot\vec{n} = -\frac{i^{ct}_{a/e}(t) + i^{dl}_{a/e}(t)}{F} \tag{66a}$$

$$\vec{h}_{Li^+}(L_e,t)\cdot\vec{n} = -\frac{i^{ct}_{e/c}(t) + i^{dl}_{e/c}(t)}{F}\,. \tag{66b}$$

Considering the non-faradaic current contribution (dis)charging the electrical double layers $i^{dl}_{\alpha}(t)$, it can be defined in derivative form as

$$i^{dl}_{\alpha}(t) = C^{dl}_{\alpha}\,\frac{\partial[\![\,\phi\,]\!]}{\partial t}, \tag{67}$$

where the jump $[\![\,\phi\,]\!]$ of the electric potential at the electrolyte/electrode interface is always defined as the electrode potential minus the electrolyte potential and $\alpha = a/e, e/c$. The faradaic current proposed in [15] emanates from charge transfer kinetics, in a form that extends Butler–Volmer equations to the mass transfer-influenced conditions [47]. The expression of i^{ct}_{α} at the interfaces are:

$$i^{ct}_{a/e} = i^{0}_{a/e}\left(\frac{c_{Li}(0,t)}{\bar{c}_{Li}}\exp\left[\frac{\alpha_a F}{RT}\,\eta_a(t)\right]\right.$$

$$-\frac{c_{\mathrm{Li}^+}(0,t)}{\bar{c}_{\mathrm{Li}^+}}\exp\left[-\frac{(1-\alpha_a)F}{RT}\,\eta_a(t)\right]\Bigg)\,, \tag{68a}$$

$$i_{e/c}(t)=i^0_{e/c}\left(\exp\left[\frac{\alpha_c F}{RT}\,\eta_c(t)\right]-\exp\left[-\frac{(1-\alpha_c)F}{RT}\,\eta_c(t)\right]\right)\,, \tag{68b}$$

where $\bar{c}_{\mathrm{Li}^+}$ is the average bulk concentration of species Li^+, $\bar{c}_{Li}$ is the bulk activity of the metallic Li, α_a and α_c are the charge transfer coefficients for reaction Eq. (60) and for reaction Eq. (61) respectively. The overpotentials η_a and η_c of the charge transfer reactions at the negative and positive electrode respectively are the difference between the jump $[\![\,\phi\,]\!]$ of the electric potential at the electrolyte/electrode interface (always defined as the electrode potential minus the electrolyte potential) and the open circuit potential (OCP) measured experimentally. The exchange current i^0_α are given by:

$$i^0_{a/e}=F\,k_2\,(\bar{c}_{\mathrm{Li}^+})^{\alpha_a}\,(\bar{c}_{\mathrm{Li}})^{1-\alpha_a}\,, \tag{69a}$$

$$i^0_{e/c}=F\,k_1\,c^{sat}_{\mathrm{Li}^\oplus}\left(1-\frac{\bar{c}_{\mathrm{Li}^\oplus}}{c^{sat}_{\mathrm{Li}^\oplus}}\right)^{\alpha_c}\left(\frac{\bar{c}_{\mathrm{Li}^\oplus}}{c^{sat}_{Li^\oplus}}\right)^{1-\alpha_c}\left(\bar{c}_{\mathrm{Li}^+}\right)^{\alpha_c}\,, \tag{69b}$$

with k_2 and k_1 the standard rate constants for reactions Eqs. (60) and (61), respectively. The reader may refer to [15] for further details on these equations and on the geometric capacitance. In view of the splitting of lithium flux in interstitial and hopping, faradaic interface conditions split, too:

$$i^{ct}_{a/e}=i^{ct}_{a/e_{\mathrm{Li}^+}}+i^{ct}_{a/e_{\mathrm{Li}^+_{\mathrm{hop}}}}\,,\qquad i^{ct}_{e/c}=i^{ct}_{e/c_{\mathrm{Li}^+}}+i^{ct}_{e/c_{\mathrm{Li}^+_{\mathrm{hop}}}} \tag{70}$$

with the interstitial and hopping contributions to charge transfer current clearly identified. They can be inferred from Butler–Volmer Eqs. (68). The exchange currents read:

$$\begin{aligned}
i^0_{a/e_{\mathrm{Li}^+}}&=F\,k_2\,(\bar{c}_{\mathrm{Li}^+})^{\alpha}\,(\bar{c}_{\mathrm{Li}})^{1-\alpha}\,,\\
i^0_{e/c_{\mathrm{Li}^+}}&=F\,k_1\,c^{sat}_{\mathrm{Li}^\oplus}\left(1-\frac{\bar{c}_{\mathrm{Li}^\oplus}}{c^{sat}_{\mathrm{Li}^\oplus}}\right)^{\alpha}\left(\frac{\bar{c}_{\mathrm{Li}^\oplus}}{c^{sat}_{\mathrm{Li}^\oplus}}\right)^{1-\alpha}(\bar{c}_{\mathrm{Li}^+})^{\alpha}
\end{aligned} \tag{71a}$$

$$\begin{aligned}
i^0_{a/e_{\mathrm{Li}^+_{\mathrm{hop}}}}&=i^0_{a/e_{\mathrm{Li}^+}}\left(\frac{\bar{c}_{\mathrm{Li}^+_{\mathrm{hop}}}}{\bar{c}_{\mathrm{Li}^+}}\right)^{\alpha}\,,\\
i^0_{e/c_{\mathrm{Li}^+_{\mathrm{hop}}}}&=i^0_{e/c_{\mathrm{Li}^+}}\left(\frac{\bar{c}_{\mathrm{Li}^+_{\mathrm{hop}}}}{\bar{c}_{\mathrm{Li}^+}}\right)^{\alpha}\,.
\end{aligned} \tag{71b}$$

where $\bar{c}_{\mathrm{Li}^+}$, $\bar{c}_{\mathrm{Li}^+_{\mathrm{hop}}}$ are average bulk concentrations of species Li^+ and $\mathrm{Li}^+_{\mathrm{hop}}$, respectively. Note that, differently from [15], those averages are not time independent. Lacking more clear understanding, we assume that the non faradaic current $i^{dl}_\alpha(t)$ as in Eq. (67) is proportional to the faradaic splitting, i.e.

$$i^{dl}_s=i^{dl}_{s\ \mathrm{Li}^+}+i^{dl}_{s\ \mathrm{Li}^+_{\mathrm{hop}}}\,, \tag{72a}$$

$$\begin{aligned}
i^{dl}_{s\ \mathrm{Li}^+}&=\frac{i^{ct}_{s\ \mathrm{Li}^+}}{i^{ct}_s}\,c^{dl}_s\,\frac{\partial[\![\,\phi\,]\!]}{\partial t}\,,\\
i^{dl}_{s\ \mathrm{Li}^+_{\mathrm{hop}}}&=\frac{i^{ct}_{s\ \mathrm{Li}^+_{\mathrm{hop}}}}{i^{ct}_s}\,c^{dl}_s\,\frac{\partial[\![\,\phi\,]\!]}{\partial t}\,,
\end{aligned} \tag{72b}$$

where the jump $[\![\,\phi\,]\!]$ of the electric potential at the electrolyte/electrode interface is always defined as the electrode potential minus the electrolyte potential and $s=a/e,e/c$. The Neumann conditions on fluxes at the left and right boundaries of the electrolyte eventually read:

$$\begin{aligned}
\vec{h}_{\mathrm{Li}^+}(0,t)\cdot\vec{n}&=-(i^{ct}_{a/e_{\mathrm{Li}^+}}+i^{dl}_{a/e_{\mathrm{Li}^+}})/F\,,\\
\vec{h}_{\mathrm{Li}^+}(L_e,t)\cdot\vec{n}&=-(i^{ct}_{e/c_{\mathrm{Li}^+}}+i^{dl}_{e/c_{\mathrm{Li}^+}})/F\,,
\end{aligned} \tag{73a}$$

$$\begin{aligned}
\vec{h}_{\mathrm{Li}^+_{\mathrm{hop}}}(0,t)\cdot\vec{n}&=-(i^{ct}_{a/e_{\mathrm{Li}^+_{\mathrm{hop}}}}+i^{dl}_{a/e_{\mathrm{Li}^+_{\mathrm{hop}}}})/F\,,\\
\vec{h}_{\mathrm{Li}^+_{\mathrm{hop}}}(L_e,t)\cdot\vec{n}&=-(i^{ct}_{e/c_{\mathrm{Li}^+_{\mathrm{hop}}}}+i^{dl}_{e/c_{\mathrm{Li}^+_{\mathrm{hop}}}})/F\,.
\end{aligned} \tag{73b}$$

The charge transfer faradaic current i^{ct} and the double layer i^{dl} currents flowing at the interfaces, described by Eqs. (70)–(72), are shown in Fig. 20 at different C-rates. The results account for the splitting of lithium flux in interstitial and hopping.

The left column collects the evolution in time of the charge transfer faradaic current i^{ct}, at the a/e and e/c interfaces. At $t=0$ all currents vanish, in view of the thermodynamic equilibrium. The charge flow ramps up according to Eq. (62) and rapidly reaches a steady state, which is maintained in time. The hopping current $i^{ct}{}_{\mathrm{Li}^+_{\mathrm{hop}}}$ is smaller than the corresponding interstitial at both interfaces, while their sum equals $i_{bat}(t)$ since $i^{dl}_{a/e}$ and $i^{dl}_{e/c}$ are vanishing after a short time.

The non-faradaic currents $i^{dl}_{a/e}$ and $i^{dl}_{e/c}$ are plot in the right columns of Fig. 20 at different C-rates. The anodic double layer current is basically null throughout the discharge time, whereas the cathodic one reaches soon its maximum value, (still several order of magnitude smaller than i^{ct}), and returns to zero at similar speed.

Currents and mass fluxes are related by the Faraday's constant F. The mass fluxes of the two species of lithium across the electrolyte, $\vec{h}_{\mathrm{Li}^+}$ and $\vec{h}_{\mathrm{Li}^+_{\mathrm{hop}}}$, are given in dashed and solid line in Fig. 21 respectively. Two $C-rates$ and two sets of equilibrium constants are considered. Figs. 21a and 21b refer to the same C-rate (3.2) but to different equilibrium constants (specifically, Fig. 21a kinetic constants are the ones in italic in Table 2). Figs. 21b and 21c share the same constants but refer to the different C-rates (3.2 vs 51.2). In all three cases, the fluxes at anode and cathode remains basically unchanged in time, confirming the evidence discussed in Fig. 20. The profile across the electrolyte however evolves towards a uniform profile, which corresponds to a steady state. In all cases both interstitial and hopping fluxes are positive, hence there is no counter-flux in any of the two mechanisms and lithium flows from the anode to the cathode in discharge.

Fig. 21 highlights that the sum of the interstitial and hopping fluxes remains constant in space and time: this event is due to the electroneutrality. In fact, enforcing Eq. (11) in the linear combination of Eqs. (8)–(9), one easily gets

$$\mathrm{div}\left[\vec{h}_{\mathrm{Li}^+}+\vec{h}_{\mathrm{Li}^+_{\mathrm{hop}}}\right]=0\quad 0\le x\le L_e. \tag{74}$$

In turn, this implies that the total lithium $c^{tot}_{\mathrm{Li}^+}=c_{\mathrm{Li}^+}+c_{\mathrm{Li}^+_{\mathrm{hop}}}$ obeys the evolution equation

$$\frac{\partial c^{tot}_{\mathrm{Li}^+}}{\partial t}=w\quad 0\le x\le L_e\,, \tag{75}$$

thus highlighting the fundamental role of the ionization reaction (1) in the charge/discharge process. The hopping flux decreases from the electrodes toward the center of the electrolyte. Since the ionic flow goes from the anode to the cathode, this results in accumulation of hopping lithium at the anode and a depletion at the cathode. The interstitial lithium behaves in the opposite way and the same holds for vacancies that are not filled by the hopping lithium.

Concentrations profiles

Fig. 22 depicts the evolution of lithium concentration $c_{\mathrm{Li}^\oplus}(x)$ in the cathode and in the solid electrolyte. Since two ionic concentrations are concurrently present in the electrolyte, only their sum $(c_{\mathrm{Li}^+}+c_{\mathrm{Li}^+_{\mathrm{hop}}})$ has been plotted in Fig. 22.

The anode, made of a metallic foil of lithium, is unaffected by the lithiation/delithiation processes and considered as an unlimited reservoir of lithium. The lithium ions intercalate inside the cathode and accumulates near at the electrolyte/cathode interface. The discharge process ends when lithium in cathode reaches its saturation limit $c^{sat}_{\mathrm{Li}^\oplus}=23400\ \mathrm{mol\ m^{-3}}$. Saturation of the interface electrolyte/cathode is thus the limiting factor for the performance of this battery.

Concentrations c_{Li_0}, c_{n^-}, c_{Li^+} and $c_{\mathrm{Li}^+_{hop}}$ are plotted separately in Fig. 23. The number of uncompensated negative vacancies, balanced by the interstitial lithium, is higher at the cathode in discharge. Note that, in view of electroneutrality and of the assumption of no negative charges flow, the total concentration of lithium cannot vanish,

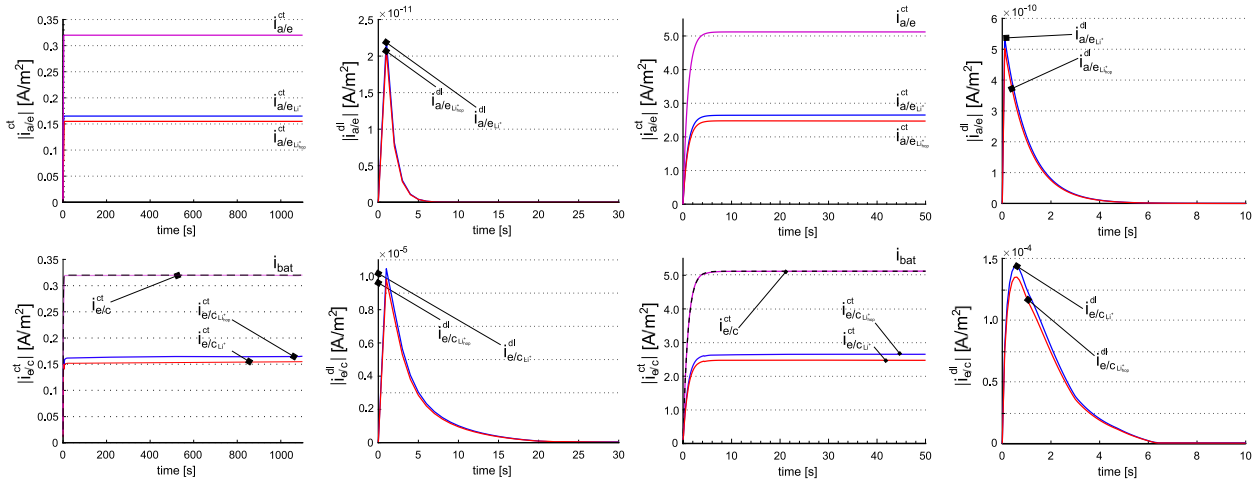

(a) $C\text{–}rate = 3.20$ (b) $C\text{–}rate = 51.2$

Fig. 20. Left (right) column: evolution in time of the charge transfer faradaic current i^{ct} (double layer current i^{dl}), at the a/e and e/c interfaces at different C-rates.

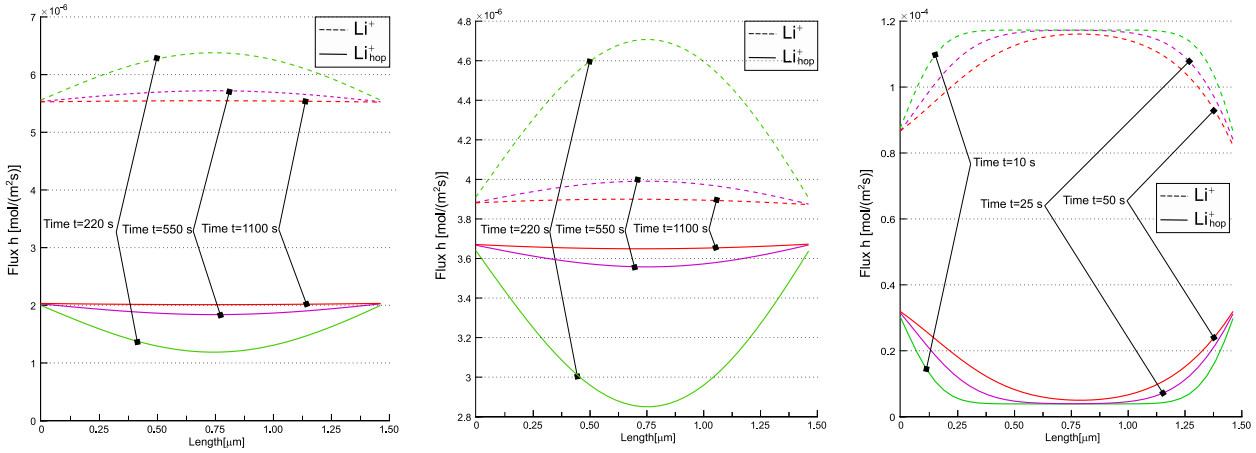

(a) Total fluxes for $C\text{–}rate = 3.2$, $K_{\text{eq}}^{\text{ion}} = 2000$ and $K_{\text{eq}}^{\text{hop}} = 0.187$.

(b) Total fluxes for $C\text{–}rate = 3.2$, $K_{\text{eq}}^{\text{ion}} = 1250$ and $K_{\text{eq}}^{\text{hop}} = 0.9$.

(c) Total fluxes for $C\text{–}rate = 51.2$, $K_{\text{eq}}^{\text{ion}} = 1250$ and $K_{\text{eq}}^{\text{hop}} = 0.9$.

Fig. 21. Interstitial and hopping lithium fluxes inside the electrolyte at different C-rates and equilibrium constants.

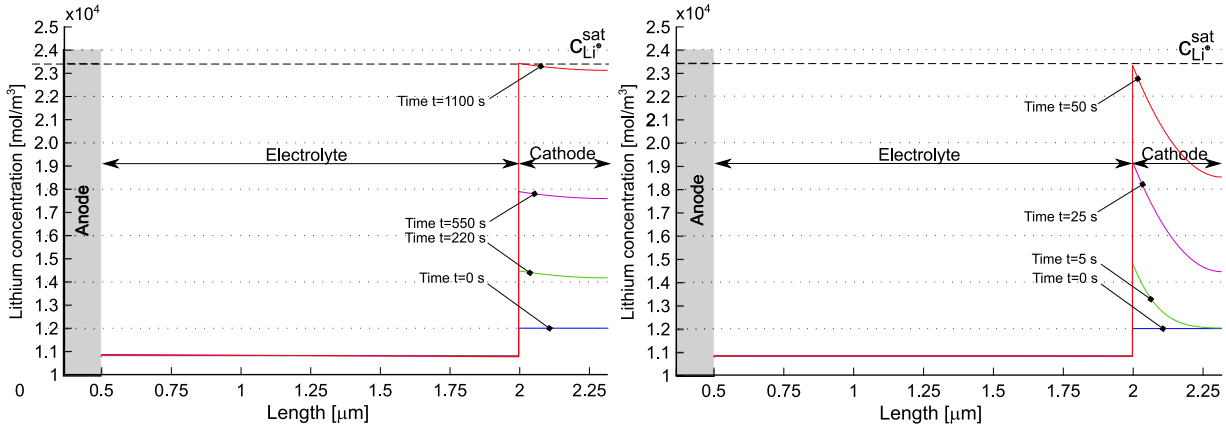

(a) $C\text{–}rate = 3.20$ (b) $C\text{–}rate = 51.2$

Fig. 22. Lithium concentration profiles inside the battery at different time steps for two different $C\text{–}rates$. The blue lines correspond to the initial time step, when the lithium concentrations inside the single components of the battery are in equilibrium and no profile is developed. The final time step, in red line, corresponds to the instant when the battery is considered discharged since the concentration of lithium $Li^{\oplus}$ inside the cathode reaches the saturation limit $c_{Li^{\oplus}}^{sat}$. (For interpretation of the references to color in this figure legend, the reader is referred to the web version of this article.)

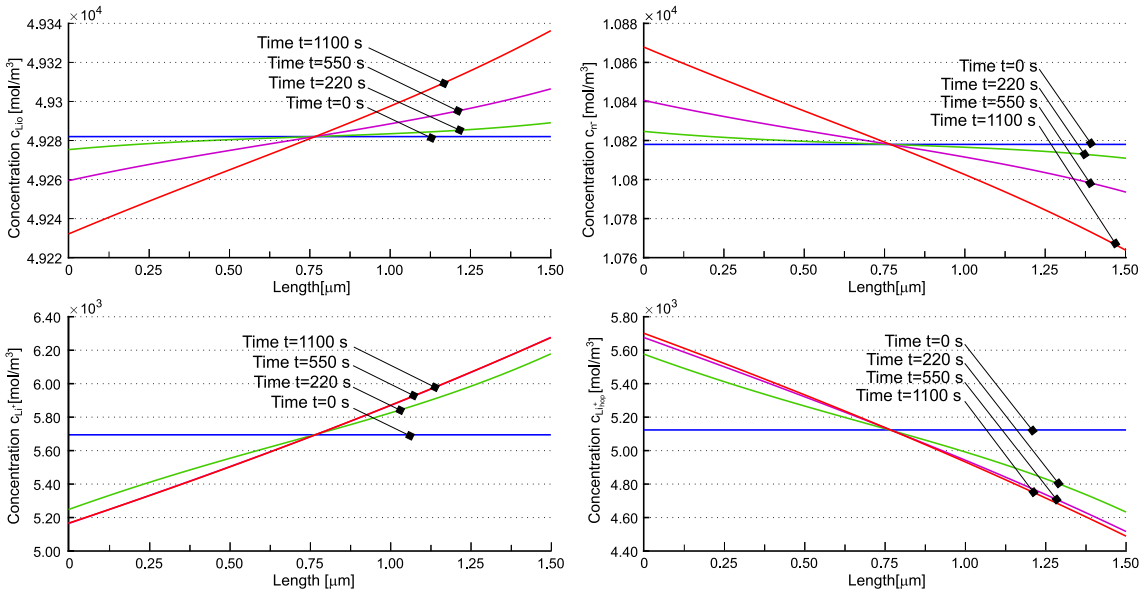

(a) $C\text{–}rate = 3.20$

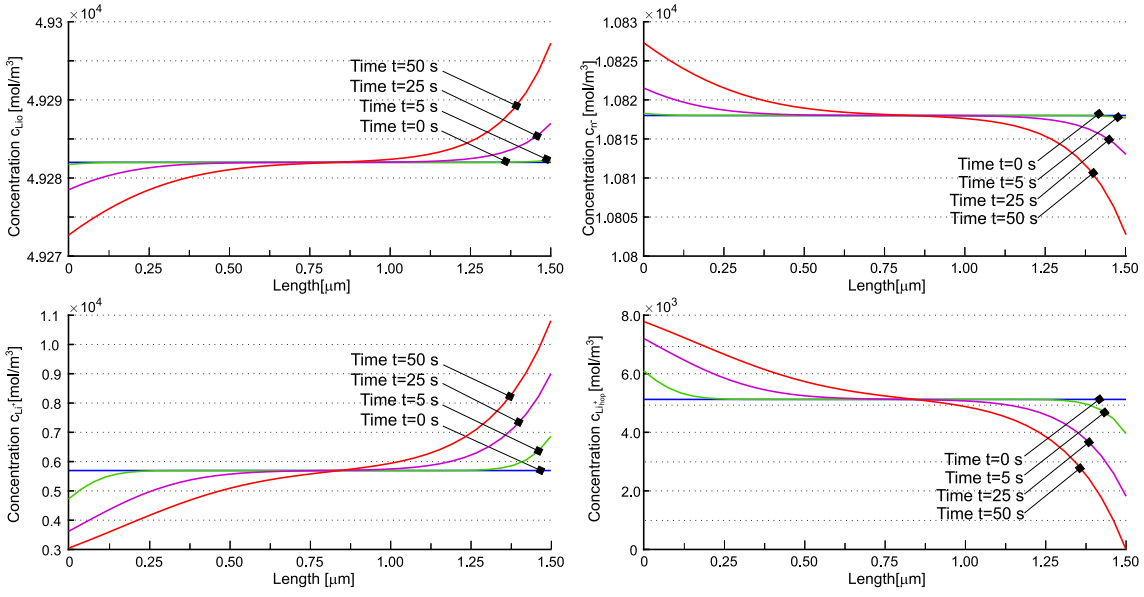

(b) $C\text{–}rate = 51.2$

Fig. 23. Lithium concentration profiles of the different species c_{Li_0}, c_{n^-}, c_{Li^+} and $c_{Li^+_{hop}}$ inside the solid electrolyte at different time steps for a $C\text{–}rate = 3.2$ (a) and a $C\text{–}rate = 51.2$ (b).

differently from liquid electrolyte and from [15]. Nonetheless, the contributions c_{Li^+} and $c_{Li^+_{hop}}$ can separately become zero (see Fig. 23(d)). The consequences of this event are yet unclear.

The concentration of $Li^{\oplus}$ in the cathode increases with the discharge time, in agreement with the Li-intercalation reaction of Eq. (61). The higher the C-rate, the steeper the expected concentration gradient, hence diffusion in the electrode may become an issue at high C-rates. At 51.2, this phenomena is clearly visible in Fig. 22(b).

The total lithium concentration at the interfaces with the two electrodes is plotted in Fig. 24. The tangent at $t = 0$ vanishes: this is explained by the resulting electroneutrality coupled to the equilibrium condition $w = 0$ imposed at $t = 0$ in Eq. (8)b. The concentrations at the two electrodes evolve according to mass balance Eqs. (9). As noticed in Fig. 21, the fluxes tend in time to achieve a uniform value across the electrolyte, i.e. the divergence term becomes less and less important and the evolution of concentrations turns out to be driven by the evolution of w. It is thus expected that, at the same equilibrium constant, increasing the reaction constant (i.e. making the reaction faster) would allow reaching the steady state in due time. This is numerically confirmed in Fig. 24, where the higher the k_f^{ion} and k_b^{ion}, keeping $K_{\text{eq}}^{\text{ion}} = 1250$, the sooner the concentration plateau is reached. Note that steady state in that case is obtained only at low C-rates.

9. Conclusions

In this note, we proposed a novel model for solid electrolytes and thoroughly investigated its electrochemical response. The model belongs to the class of *two-mechanism models*, in which the ionic motility is depicted as due to hopping and interstitial diffusion. After the ionization reactions occur, some ions hop and fill neighboring vacancies, whereas the remaining positive ions move in a meta-stable interstitial state. In this work, the dynamic filling of vacancies by neighboring positions is modeled explicitly. The concentration of negatively charged vacancies results from the solution of the governing equations.

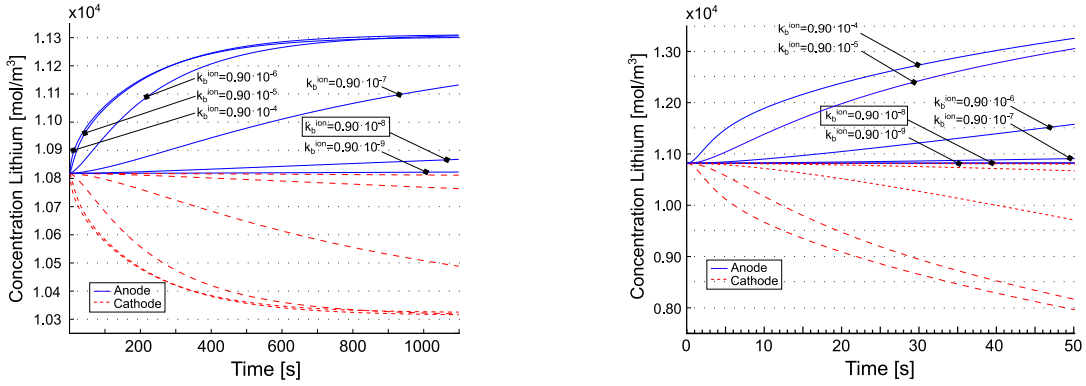

(a) $C\text{–}rate = 3.20$ (b) $C\text{–}rate = 51.2$

Fig. 24. Lithium concentration at the interfaces with the two electrodes, for two different $C\text{–}rates$. Several values for k_b^{ion} have been chosen, at constant $K_{\text{eq}}^{\text{ion}} = 1250$. The blue lines correspond to the values measured at the interface anode/electrolyte and the red line corresponds to the interface electrolyte/cathode. Note that the initial tangent vanishes: this is explained by the resulting electroneutrality coupled to the equilibrium condition $w = 0$ imposed at $t = 0$ in Eq. (8)b. (For interpretation of the references to color in this figure legend, the reader is referred to the web version of this article.)

Mass balance equations, chemical kinetics laws, balance of momentum, and Ampere's law are framed in the rigorous setting of the thermo-chemo-mechanics of continua. The model is fully three-dimensional and, in order to ensure the multiscale compatibility, depicts the electric field by means of the quasi-static Ampere–Maxwell equations, without imposing electroneutrality a priori [17].

Governing equations have been either solved numerically via the finite element method or analytically, in seeking for the steady state solution. Interface currents, the electric potential, fluxes and concentrations profiles have been analyzed at equilibrium, steady state, and time-dependent behaviors. The transient response shows a non-uniform profile of ionic concentrations, with gradients that attenuate in time towards a uniform ionic distribution at steady state. Depending upon the material parameters and initial conditions, the time required to complete the transient phase turned out to be extremely long; as a consequence, the transient response might even be the only relevant behavior during real life battery operations.

The simulations outcomes have been validated against the experimental evidence presented in [15] and in [18]. Quantities of interest, as discharge curves, agree well across the wide range of investigated $C - rates$.

The model sensitivity on the material parameters was investigated, too, with the aim of identifying the ones that contribute the most to the response. It turned out that the most relevant parameter is the fraction of Li that resides in equilibrium in the mobile state, which can be accurately estimated according to [15].

Further developments of the proposed framework are in progress, with the aim of accounting for multi-physics interactions and realistic descriptions of the microstructure of composite cells. The processes within the proposed model are in fact described as isothermal, although it is quite well known, at least in liquid electrolytes, that temperature affects the response of batteries [43]. Furthermore, the volume of electrodes changes with cycling, due to repeated insertion and removal of Li atoms, causing disconnection and reduced contacts. In our simulations, though, the active surface area, where redox processes occur, was unaltered over cycling. All above assumptions are going to be removed in our future research efforts.

CRediT authorship contribution statement

L. Cabras: Conception and design of study, Acquisition of data, Analysis and/or interpretation of data, Writing – original draft, Revising the manuscript critically for important intellectual content. **D. Danilov:** Acquisition of data, Analysis and/or interpretation of data, Revising the manuscript critically for important intellectual content. **W. Subber:** Analysis and/or interpretation of data, Writing – original draft, Revising the manuscript critically for important intellectual content. **V. Oancea:** Conception and design of study, Analysis and/or interpretation of data, Revising the manuscript critically for important intellectual content. **A. Salvadori:** Conception and design of study, Acquisition of data, Analysis and/or interpretation of data, Writing – original draft, Revising the manuscript critically for important intellectual content.

Declaration of competing interest

The authors declare that they have no known competing financial interests or personal relationships that could have appeared to influence the work reported in this paper.

Acknowledgment

All authors approved the final version of the manuscript.

Appendix. Equilibrium conditions for the chemical reactions

Equilibrium conditions for the chemical reactions (1) and (3) can be achieved from thermodynamics, as well. Imposing a vanishing affinity for (3), for instance, leads to

$$A^y = \overline{\mu}_{\text{Li}^+_{\text{hop}}} - \overline{\mu}_{\text{Li}^+} = \mu_{\text{Li}^+_{\text{hop}}} - \mu_{\text{Li}^+} = 0 \tag{76}$$

in view of definition (35b) since hopping and interstitial flows share the same electric potential. For ideal solutions, replacing Eq. (37) into Eq. (76), it comes out

$$\mu^0_{\text{Li}^+_{\text{hop}}} - \mu^0_{\text{Li}^+} = RT \log \frac{c^{\text{eq}}_{\text{Li}^+_{\text{hop}}}}{c^{\text{eq}}_{\text{Li}^+}} = RT \log K^{\text{hop}}_{\text{eq}} \tag{77}$$

by setting $y = 0$ into Eq. (6b). Eq. relates $K^{\text{hop}}_{\text{eq}}$ to the negative of the Gibbs free energy change $\mu^0_{\text{Li}^+_{\text{hop}}} - \mu^0_{\text{Li}^+}$. The thermodynamic restriction

$$y\, A^y \le 0$$

is satisfied using Eq. (6b). The affinity and the reaction rate can be restated as:

$$A^y = RT \ln \left[\frac{\theta_{\text{Li}^+_{\text{hop}}}}{1-\theta_{\text{Li}^+_{\text{hop}}}} \frac{1-\theta_{\text{Li}^+}}{\theta_{\text{Li}^+}} \frac{1}{K^{\text{hop}}_{\text{eq}}} \right],$$

$$y = k_b^{\text{hop}} \left\{ -\frac{\theta_{\text{Li}^+_{\text{hop}}}}{1-\theta_{\text{Li}^+_{\text{hop}}}} + \frac{\theta_{\text{Li}^+}}{1-\theta_{\text{Li}^+}} K^{\text{hop}}_{\text{eq}} \right\}.$$

If $y > 0$ then

$$K_{eq}^{hop} > \frac{\theta_{Li^+_{hop}}}{1-\theta_{Li^+_{hop}}} \frac{1-\theta_{Li^+}}{\theta_{Li^+}}$$

and in turn $A^y < 0$. Viceversa if $y < 0$ then $A^y > 0$.

References

[1] J. Schnell, T. Günther, T. Knoche, C. Vieider, L. Köhler, A. Just, M. Keller, S. Passerini, G. Reinhart, All-solid-state lithium-ion and lithium metal batteries – paving the way to large-scale production, J. Power Sources 382 (2018) 160–175.

[2] F. Zheng, M. Kotobuki, S. Song, M. Lai, L. Lu, Review on solid electrolytes for all-solid-state lithium-ion batteries, J. Power Sources 389 (2018) 198–213.

[3] D. Bistri, A. Afshar, C.V. Di Leo, Modeling the chemo-mechanical behavior of all-solid-state batteries: a review, Meccanica (2020).

[4] M. Ganser, F.E. Hildebrand, M. Kamlah, R.M. McMeeking, A finite strain electro-chemo-mechanical theory for ion transport with application to binary solid electrolytes, J. Mech. Phys. Solids 125 (2019) 681–713.

[5] C.V. Di Leo, E. Rejovitzky, L. Anand, Diffusion-deformation theory for amorphous silicon anodes: the role of plastic deformation on elecrochemical performance, Int. J. Solids Struct. 67–68 (2015) 283–296.

[6] H. Fathiannasab, A.G. Kashkooli, T. Li, L. Zhu, Z. Chen, Three-dimensional modeling of all-solid-state lithium-ion batteries using synchrotron transmission X-ray microscopy tomography, J. Electrochem. Soc. 167 (10) (2020) 100558.

[7] H. Fathiannasab, L. Zhu, Z. Chen, Chemo-mechanical modeling of stress evolution in all-solid-state lithium-ion batteries using synchrotron transmission X-ray microscopy tomography, J. Power Sources 483 (2021) 229028.

[8] A. Salvadori, P.A. Wawrzynek, F. Fantoni, Fracture propagation in brittle materials as a standard dissipative process: Effective crack tracking algorithms based on a viscous regularization, J. Mech. Phys. Solids 127 (2019) 221–238.

[9] A. Salvadori, F. Fantoni, Minimum theorems in 3D incremental linear elastic fracture mechanics, INT J FRACTURE 184 (1) (2013) 57–74.

[10] A. Salvadori, F. Fantoni, Fracture propagation in brittle materials as a standard dissipative process: general theorems and crack tracking algorithms., J. Mech. Phys. Solids 95 (2016) 681–696.

[11] S.D. Fabre, D. Guy-Bouyssou, P. Bouillon, F. Le Cras, C. Delacourt, Charge/discharge simulation of an all-solid-state thin-film battery using a one-dimensional model, J. Electrochem. Soc. 159 (2) (2012) A104–A115.

[12] A. Salvadori, D. Grazioli, M.G.D. Geers, Governing equations for a two-scale analysis of Li-ion battery cells, Int. J. Solids Struct. 59 (2015) 90–109.

[13] D. Li, D.L. Danilov, J. Xie, L. Raijmakers, L. Gao, Y. Yang, P.H.L. Notten, Degradation mechanisms of C6/LiFePO4 batteries: experimental analyses of calendar aging, Electrochim. Acta 190 (2016) 1124–1133.

[14] D. Li, D.L. Danilov, L. Gao, Y. Yang, P.H.L. Notten, Degradation mechanisms of C6/LiFePO4 batteries: experimental analyses of cycling-induced aging, Electrochim. Acta 210 (2016) 445–455.

[15] L.H.J. Raijmakers, D.L. Danilov, R.A. Eichel, P.H.L. Notten, An advanced all-solid-state Li-ion battery model, Electrochim. Acta 330 (135147) (2020).

[16] G. Li, C.W. Monroe, Multiscale lithium-battery modeling from materials to cells, Annu. Rev. Chem. Biomol. 11 (1) (2020) 277–310.

[17] A. Salvadori, D. Grazioli, M.G.D. Geers, D. Danilov, P.H.L Notten, A multiscale-compatible approach in modeling ionic transport in the electrolyte of (Lithium ion) batteries, J. Power Sources 293 (2015) 892–911.

[18] D. Danilov, R.A.H. Niessen, P.H.L. Notten, Modeling all-solid-state Li-ion batteries, J. Electrochem. Soc. 158 (3) (2011) A215–A222.

[19] A. Bonnefont, F. Argoul, M.Z. Bazant, Analysis of diffuse-layer effects on time-dependent interfacial kinetics, J. Electr. Chem. 500 (1) (2001) 52–61.

[20] M. Landstorfer, S. Funken, T. Jacob, An advanced model framework for solid electrolyte intercalation batteries, Phys. Chem. Chem. Phys. 13 (2011) 12817–12825.

[21] A. Salvadori, D. Grazioli, M. Magri, M.G.D. Geers, D. Danilov, P.H.L. Notten, On the role of saturation in modeling ionic transport in the electrolyte of (Li-ion) batteries, J. Power Sources 294 (2015) 696–710.

[22] A. Bielefeld, D.A. Weber, J. Janek, Microstructural modeling of composite cathodes for all solid state batteries, J. Phys. Chem. C 123 (2019) 1626–1634.

[23] A. Saltelli, S. Tarantola, F. Campolongo, M. Ratto, Sensitivity Analysis in Practice: A Guide To Assessing Scientific Models, Vol. 1, Wiley Online Library, 2004.

[24] A. Salvadori, R.M. McMeeking, D. Grazioli, M. Magri, A coupled model of transport-reaction-mechanics with trapping. Part I - small strain analysis, J. Mech. Phys. Solids 114 (2018) 1–30.

[25] S.R. De Groot, P. Mazur, Non-Equilibrium Thermodynamics, Dover, 1984.

[26] J. Newman, K.E. Thomas-Alyea, Electrochemical Systems, John Wiley and Sons B.V., 2004.

[27] M. Doyle, T.F. Fuller, J. Newman, Modeling of galvanostatic charge and discharge of the lithium/polymer/insertion cell, J. Electrochem. Soc. 140 (1993) 1526–1533.

[28] R.E. Garcia, Y.M. Chiang, W.C. Carter, P. Limthongkul, C.M. Bishop, Microstructural modeling and design of rechargeable lithium-ion batteries, J. Electrochem. Soc. 152 (2005) 255–263.

[29] C.W. Wang, A.M. Sastry, Mesoscale modeling of a Li-ion polymer cell, J. Electrochem. Soc. 154 (2007) A1035–A1047.

[30] S. Golmon, K. Maute, M.L. Dunn, Numerical modeling of electrochemical-mechanical interactions in lithium polymer batteries, Comput. Struct. 87 (2009) 1567–1579.

[31] J. Christensen, Modeling diffusion-induced stress in Li-ion cells with porous electrodes, J. Electrochem. Soc. 157 (2010) 366–380.

[32] S. Renganathan, G. Sikha, S. Santhanagopalan, R.E. White, Theoretical analysis of stresses in a lithium ion cell, J. Electrochem. Soc. 157 (2010) 155–163.

[33] S. Golmon, K. Maute, M.L. Dunn, Multiscale design optimization of lithium ion batteries using adjoint sensitivity analysis, Int. J. Numer. Meth. Eng. 92 (2012) 475–494.

[34] D. Danilov, P.H.L. Notten, Mathematical modeling of ionic transport in the electrolyte of Li-ion batteries, Electrochim. Acta 53 (2008) 5569–5578.

[35] V. Zadin, D. Danilov, D. Brandell, P.H.L. Notten, A. Aabloo, Finite element simulations of 3D ionic transportation properties in li-ion electrodes, Electrochim. Acta 65 (2012) 165–173.

[36] T.J. Rademaker, G.R.A. Akkermans, D. Danilov, P.H.L. Notten, On the deviation of electro-neutrality in Li-ion battery electrolytes, J. Electrochem. Soc. 161 (8) (2014) E3365–E3372.

[37] P.M. Suquet, Local and global aspects in the mathematical theory of plasticity, in: A. Sawczuk, G. Bianchi (Eds.), Plasticity Today: Modeling, Methods and Applications, Elsevier Applied Science Publishers, London, 1985, pp. 279–310.

[38] M.G.D. Geers, V.G. Kouznetsova, Brekelmans W.A.M., Multi-scale computational homogenization: trends and challenges, J. Comput. Appl. Math. 234 (2010) 2175–2182.

[39] A.A. Franco, Multiscale modelling and numerical simulation of rechargeable lithium ion batteries: concepts, methods and challenges, RSC Adv. 3 (13027) (2013).

[40] A.A. Franco, M.L. Doublet, W.G.B. Bessler (Eds.), Physical multiscale modeling and numerical symulation of electrochemical devices for energy conversion and storage, Springer, London, 2016.

[41] A.A. Franco, A. Rucci, D. Brandell, C. Frayret, M. Gaberscek, P. Jankowski, P. Johansson, Boosting rechargeable batteries R&D by multiscale modeling: Myth or reality? Chem. Rev. 119 (2019) 4569.

[42] S. Dargaville, T.W. Farrell, Predicting active material utilization in $LiFePO_4$ electrodes using a multiscale mathematical model, J. Electrochem. Soc. 157 (7) (2010) A830–A840.

[43] A. Latz, J. Zausch, Multiscale modeling of li-ion batteries: thermal aspects., Beilstein J. Nanotechnol. 6 (2015) 987–1007.

[44] S. Pannala, J.A. Turner, S. Allu, W.R. Elwasif, S. Kalnaus, S. Simunovic, A. Kumar, J.J. Billings, H. Wang, J. Nada, Multiscale modeling and characterization for performance and safety of lithium-ion batteries, J Appl. Phys. 118 (2015) 072017.

[45] C. Wieser, T. Prill, K. Schladitz, Multiscale simulation process and application to additives in porous composite battery electrodes, J. Power Sources 277 (2015) 64–75.

[46] L. Zielke, T. Hutzenlaub, D.R. Wheeler, C.W. Chao, I. Manke, A. Hilger, N. Paust, R. Zengerle, S. Thiele, Three-phase multiscale modeling of a $LiCoO_2$ cathode: combining the advantages of FIB-SEM imaging and X-Ray tomography, Adv. Energy Mater. 5 (2015) 1401612.

[47] A.J Bard, L.R. Faulkner, Electrochemical Methods: Fundamentals and Applications, second ed., Wiley, 2000.

[48] R.A. Huggins, Advanced Batteries: Materials Science Aspects, Springer, 2010.

[49] L.D. Landau, L.P. Pitaevskii, E.M. Lifshitz, Electrodynamics of Continuous Media, 2nd, in: Course of Theoretical Physics, vol. 8, Elsevier, 1984.

[50] J. Larsson, Electromagnetics from a quasistatic perspective, Am. J. Phys. 75 (3) (2007) 230–239.

[51] H.A. Haus, J.R. Melcher, Electromagnetic Fields and Energy, Prentice-Hall, 1989.

[52] M.W. Swift, J.W. Swift, Y. Qi, Modeling the electrical double layer at solid-state electrochemical interfaces, Nat. Comp. Sci. 1 (3) (2021) 212–220.

[53] R. DeHoff, Thermodynamic in Material Science, CRC Press - Taylor and Francis, 2006.

[54] S. Ghosh, P. Pandita, S. Atkinson, W. Subber, Y. Zhang, N.C. Kumar, S. Chakrabarti, L. Wang, Advances in Bayesian probabilistic modeling for industrial applications, ASCE-ASME J. Risk Uncertain. Eng. Syst. B Mech. Eng. 6 (3) (2020).

[55] Y. Zhang, S. Ghosh, P. Pandita, W. Subber, G. Khan, L. Wang, Remarks for scaling up a general gaussian process to model large dataset with sub-models, in: AIAA Scitech 2020 Forum, 2020, p. 0678.

[56] M. Magri, B. Boz, L. Cabras, A. Salvadori, Quantitative investigation of the influence of electrode morphology in the electro-chemo-mechanical response of Li-ion batteries, Electrochimica Acta 405 (2021) 139778.